

# Multimodality Imaging in Evaluating and Guiding Percutaneous Left Atrial Appendage Occlusion

Renuka Jain, MD, Priscilla Wessly, MD, Muhamed Saric, MD, PhD, Karl Richardson, MD, Enrique Garcia-Sayan, MD, Karima Addetia, MD, Lauren Howard, BS, RDCS (AE, PE), RVT, Thomas Finn, BS, and Nishath Quader, MD, *Milwaukee, Wisconsin; New York, New York; Winston-Salem, North Carolina; Houston, Texas; Chicago, Illinois; and St. Louis, Missouri*

Left atrial appendage occlusion (LAAO) has emerged as an important intervention for stroke prevention in patients with nonvalvular atrial fibrillation (AF) who are unable to tolerate long-term anticoagulation. The development of advanced imaging technologies and techniques, such as three-dimensional (3D) echocardiography with multiplanar reconstruction, multidetector cardiac computed tomography (MDCT), 3D intracardiac echocardiography (ICE), 3D printing, and simulation, has revolutionized preprocedural planning, intraprocedural guidance, and postprocedural surveillance, ensuring improved precision and outcomes. Transesophageal echocardiography (TEE) remains a foundational imaging modality for assessing left atrial appendage morphology, excluding thrombi, and obtaining accurate measurements for device sizing. Recent advances in 3D TEE and multiplanar reconstruction techniques enable enhanced visualization of complex left atrial appendage anatomies, improving device selection and procedural planning. MDCT has a growing role, offering high-resolution 3D reconstructions for detailed anatomic assessment. Additionally, its applications in 3D printing and virtual device simulation provide patient-specific insights, facilitating optimal device sizing and improving procedural efficiency. Intraprocedurally, 3D ICE has gained traction as a valuable alternative to TEE. With its real-time imaging capabilities and high spatial resolution, 3D ICE allows precise guidance during transseptal puncture and device deployment while reducing the need for general anesthesia. Postprocedurally, both TEE and MDCT play critical roles in assessing device stability and identifying complications such as device-related thrombus and peridevice leak. This review highlights the evolving role of multimodality imaging in LAAO, including innovations such as 3D ICE, 3D printing, and simulation. The authors also review recent literature to establish state-of-the-art imaging practices, providing a comprehensive discussion of imaging applications across pre-, intra-, and postprocedural phases to optimize outcomes and minimize complications in LAAO. (*J Am Soc Echocardiogr* 2025; ■: ■ - ■.)

**Keywords:** Echocardiography, Left atrial appendage, Left atrial appendage occlusion, Multimodality imaging, Transesophageal echocardiography

Atrial fibrillation (AF) affects >33 million people worldwide and is the second leading cause of stroke, resulting in significant clinical morbidity.<sup>1,2</sup> Echocardiographic studies show that >90% of thrombi in nonvalvular AF form in the left atrial appendage (LAA).<sup>3</sup>

From the Aurora Cardiovascular and Thoracic Services, Aurora Sinai/Aurora St. Luke's Medical Centers, Milwaukee, Wisconsin (R.J., P.W., L.H., T.F.); Division of Cardiovascular Medicine, University of Wisconsin School of Medicine and Public Health, Milwaukee, Wisconsin (R.J.); Leon H. Charney Division of Cardiology, New York University Langone Health, New York, New York (M.S.); Department of Cardiovascular Medicine, Atrium Health Wake Forest Baptist Medical Center, Winston-Salem, North Carolina (K.R.); Section of Cardiology, Department of Medicine, Texas Heart Institute at Baylor College of Medicine, Houston, Texas (E.G.-S.); Section of Cardiology, University of Chicago Heart & Vascular Center, Chicago, Illinois (K.A.); and Division of Cardiovascular Medicine, Washington University in St. Louis, St. Louis, Missouri (N.Q.).

Reprint requests: Renuka Jain, MD, Aurora Cardiovascular and Thoracic Services, Aurora St. Luke's Medical Center, 2801 W Kinnickinnic River Parkway, Suite 130, Milwaukee, WI 53215 (E-mail: [wi.publishing159@aaah.org](mailto:wi.publishing159@aaah.org)).

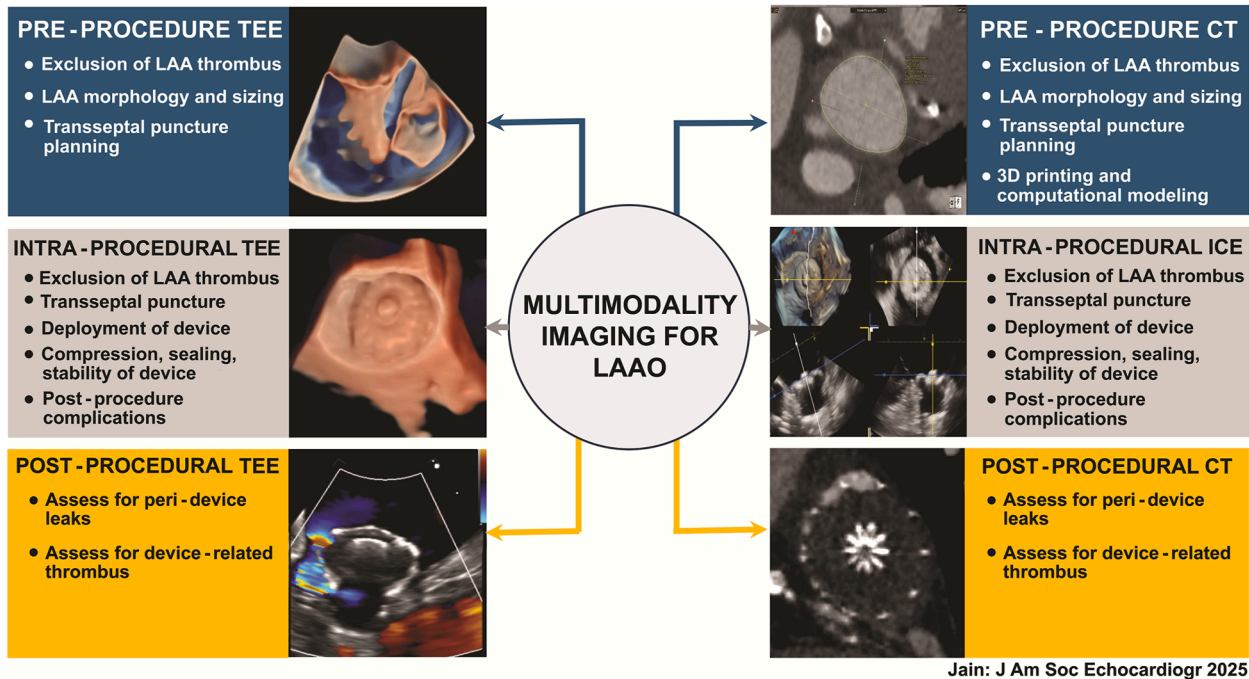
0894-7317/\$36.00

Copyright 2025 by the American Society of Echocardiography.

<https://doi.org/10.1016/j.echo.2025.07.009>

Anticoagulation therapy significantly reduces the risk for ischemic stroke and all-cause mortality. However, >50% of eligible patients either discontinue or avoid anticoagulants because of bleeding concerns, side effects, or noncompliance.<sup>4</sup> Alternative strategies for stroke prevention are therefore needed. The concept of LAA exclusion dates to 1949, when John L. Madden performed surgical resection to prevent recurrent arterial thrombi.<sup>5</sup> Surgical LAA exclusion strategies offered a viable option for patients unable to tolerate long-term anticoagulation, but evidence of efficacy was limited.

The PROTECT AF (Watchman Left Atrial Appendage System for Embolic Protection in Patients With Atrial Fibrillation)<sup>6</sup> and PREVAIL (Watchman LAA Closure Device in Patients With Atrial Fibrillation Versus Long Term Warfarin Therapy)<sup>7,8</sup> trials demonstrated that percutaneous LAA occlusion (LAAO) device implantation was noninferior to warfarin for stroke prevention in nonvalvular AF. The approval of the first pluglike transcatheter LAAO device (with a single occlusive mechanism) in 2015 marked a milestone in LAAO therapy. In 2021, the US Food and Drug Administration approved a second device, a disk-and-lobe system (a dual occlusive mechanism) that was shown in the Amulet IDE (Amplatzer Amulet LAA Occluder) trial<sup>9</sup> to have noninferior efficacy, further expanding the available stroke prevention options (Figure 1).



**Central Illustration** Utility of multimodality imaging for LAAO.

Abbreviations
<b>2D</b> = Two-dimensional
<b>3D</b> = Three-dimensional
<b>AF</b> = Atrial fibrillation
<b>CT</b> = Computed tomography
<b>DRT</b> = Device-related thrombus
<b>HAT</b> = Hypoattenuated thickening
<b>ICE</b> = Intracardiac echocardiography
<b>LAA</b> = Left atrial appendage
<b>LAAO</b> = Left atrial appendage occlusion
<b>MDCT</b> = Multidetector cardiac computed tomography
<b>MPR</b> = Multiplanar reconstruction
<b>PDL</b> = Peridevice leak
<b>SEC</b> = Spontaneous echocardiographic contrast
<b>TEE</b> = Transesophageal echocardiography

LAA size, shape, and relationship with surrounding structures vary significantly among patients, and these anatomic differences influence the success of LAAO procedures. Transesophageal echocardiography (TEE) has traditionally been used to evaluate LAA morphology, guide LAAO procedures, and monitor postimplantation outcomes. Recently, real-time three-dimensional (3D) intracardiac echocardiography (ICE) has gained popularity for LAAO guidance, offering imaging with high spatial and temporal resolution. Multidetector cardiac computed tomography (MDCT) has emerged as a key tool in preprocedural planning, providing detailed 3D reconstructions that allow accurate device sizing and visualization of complex LAA anatomy.

The aim of this review is to explore the role of multimodality imaging in preprocedural evaluation, intraprocedural guidance, and postprocedural follow-up in percutaneous LAAO (**Central**

**Illustration**). We also address the use of imaging in assessing device-related complications during follow-up and highlight the latest advances in and future directions of this evolving field.

## PREPROCEDURAL EVALUATION

### TEE

TEE served as the primary imaging modality in pivotal clinical trials.<sup>7,9,10</sup> Accurate image acquisition is operator dependent, and adherence to a comprehensive protocol is crucial for reliable measurements and conclusions.<sup>11</sup> The goals of TEE in the context of screening and planning for percutaneous LAAO procedures are to determine LAA morphology, exclude LAA thrombus, and perform measurements of the landing zone, thereby facilitating optimal device selection and sizing. A thorough transesophageal echocardiographic examination is recommended to evaluate left ventricular size and function, aortic plaque, aortic or mitral valve pathology (especially mitral stenosis), pericardial effusion, intracardiac masses, and the atrial septum. Baseline TEE should particularly evaluate for mitral stenosis, a marker of valvular AF, to ensure eligibility by identifying patients excluded from trials like PROTECT AF and PREVAIL. The role of percutaneous LAAO for valvular AF is currently unknown, with clinical equipoise persisting regarding its efficacy.<sup>6-8</sup> Atrial septal defects, atrial septal aneurysms, and existing atrial occluder devices may all present challenges or contraindications to the procedure.

On two-dimensional (2D) TEE, the LAA is typically imaged at four omniplane angles in 45-degree intervals (0°, 45°, 90°, and 135°) with and without color Doppler. Color flow Doppler imaging

**HIGHLIGHTS**

- Advanced imaging technologies and techniques have revolutionized LAAO.
- Three-dimensional TEE and MPR aid device sizing and procedural planning.
- MDCT allows 3D printing and virtual device simulation useful during planning.
- Three-dimensional ICE can guide transseptal puncture and device deployment.
- Postprocedure, TEE and MDCT can assess device stability and complications.

can reveal areas with decreased or absent color flow within the appendage, which is highly suggestive of thrombi. Dedicated and zoomed images are recommended for improved accuracy. The shape of the LAA is determined by the number and location of appendage lobes. A “windsock” morphology is characterized by a prominent single lobe, a “cactus” morphology by two roughly equal lobes, a “chicken wing” morphology by a lobe that arises at an acute angle from the LAA ostium (anterior or posterior to the ostium), and a “cauliflower” or “broccoli” morphology by multiple lobes and variable depth (Figure 2). These morphologies influence device selection and success. Although 2D imaging can be used to determine LAA morphology, 3D echocardiography with a zoom volume acquisition of the LAA provides a more accurate depiction of the shape, number, and location of lobes. New 3D rendering algorithms, such as light-source manipulation and transillumination technologies, can enhance visualization of the LAA morphology and allow orientation of the images to resemble fluoroscopic views (Figure 2).<sup>12,13</sup> Both the 3D LAA multiview and tilt-up-and-turn-left maneuvers are algorithms developed in stepwise fashion to assess LAA morphology in three dimensions (Figures 3 and 4).

For the pluglike LAAO device, key measurements include the landing zone, with the ostium width measured as the distance from the left circumflex coronary artery extending radially to the opposing limbus, often approximating 2 cm from the tip of the limbus (Figure 5, A). The maximum width of the anticipated landing zone is determined and used for device sizing according to the manufacturer’s recommendations. The measured landing zone must be between 14 and 36 mm to accommodate the Watchman FLX/PRO device (Boston Scientific). LAA depth is measured from the center of the anticipated landing zone to the LAA apex and should be >50% of the labeled device diameter.

For the disk-and-lobe LAAO device, the LAA orifice should be measured to ensure it is smaller than the anticipated diameter of the device disk. The anticipated landing zone of the device lobe is measured 10 to 12 mm distal to the LAA orifice, defined as the plane extending from the tip of the limbus to a location just proximal to the left circumflex coronary artery. The measured landing zone must be between 11 and 31 mm and is used for device sizing, as determined by the device manufacturer. The LAA depth is measured from the center of the LAA orifice ostium and then perpendicular to the length of the LAA orifice. Figure 5, B demonstrates the 2D LAA sizing measurements for the Amplatzer Amulet device (Abbott Cardiovascular).

For both device styles, the manufacturers’ recommendations and instructions for use suggest 2D measurements at the four omniplane angles. However, 2D measurements of a 3D orifice can lead to uncertainty about the exact plane of measurement and potential underestimation if not centered in the orifice. Three-dimensional echocardiography with multiplanar reconstruction (MPR) can provide precise measurements of the orifice and landing zone, ensuring all measurements are performed in the same plane. This approach also allows visualization of the deepest lobe and has been shown to lead to more accurate device sizing (Figure 6).<sup>14,15</sup>

**MDCT**

MDCT has a growing role in preprocedural planning for LAAO procedures because of its excellent spatial resolution and ability to

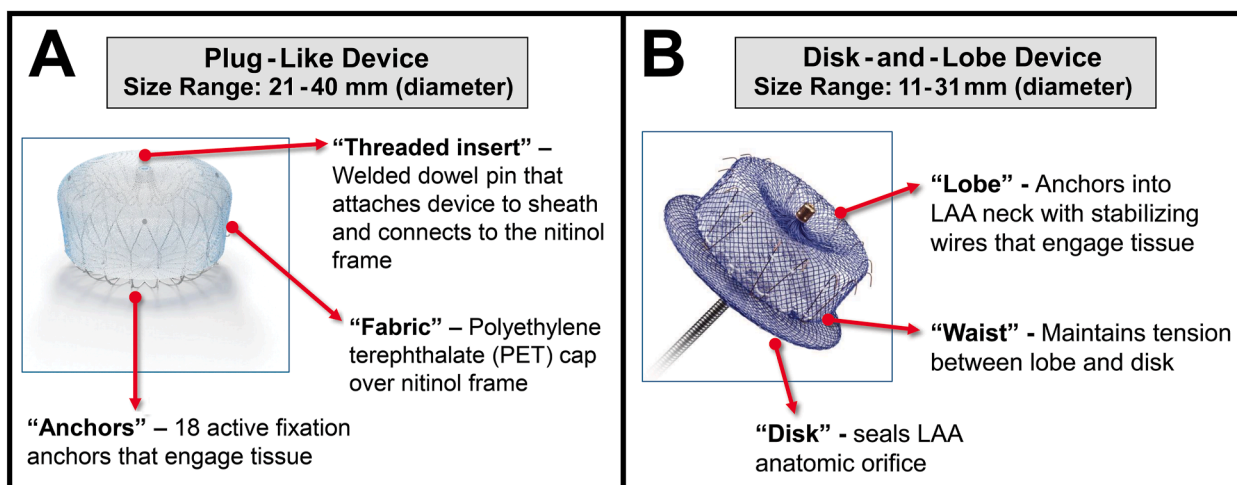


**Figure 1** Commercially approved percutaneous LAAO devices. (A) Pluglike device: This is a self-expanding Nitinol device equipped with dual-row precision fixation anchors for enhanced stability. It features a low-profile threaded insert covered by polyethylene terephthalate fabric and is available in six sizes (20–40 mm). (B) Disk-and-lobe device: Composed of a self-expanding Nitinol mesh, this device forms a lobe and a disk, connected by a central waist. It is available in eight sizes (11–31 mm). Device images are used with permission from Boston Scientific and Abbott Cardiovascular.



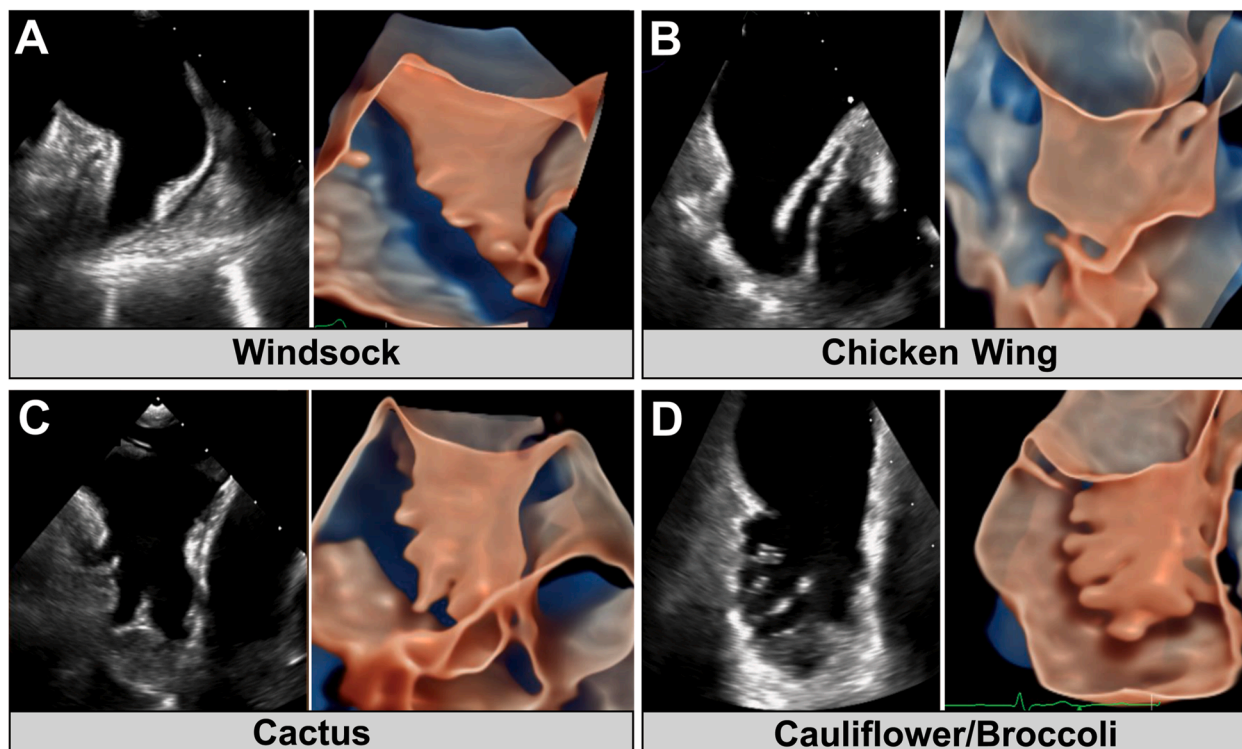


**Figure 2** LAA morphologies illustrated on 2D and 3D TEE. **(A)** Windsock, **(B)** chicken wing, **(C)** cactus, and **(D)** cauliflower or broccoli LAA morphologies are demonstrated in two dimensions (*left side of each panel*) and three dimensions. Three-dimensional TEE uses light-source manipulation and transillumination technology to provide high-definition, photorealistic, 3D volume-rendered images of the LAA.

generate precise, high-quality 3D measurements. It can replicate the key aspects of TEE in evaluating LAA morphology, maximum ostial diameter, and depth for device selection and eligibility ([Central Illustration](#)). Increasingly, MDCT is recognized as a primary imaging modality for LAAO planning, often reducing the need for preprocedural TEE. In many centers, patients may undergo TEE only at the time of device implantation, whereas in others, LAAO may be performed using ICE-guided deployment. Filby *et al.*<sup>16</sup> demonstrated that preprocedural planning guided by cardiac computed tomography (CT), in combination with ICE-guided device deployment achieved a 97.2% accuracy in device sizing and 100% procedural success in 71 patients, supporting the feasibility of non-TEE workflows with comparable outcomes. This shift underscores MDCT's ability to provide comprehensive anatomic and functional data, facilitating efficient procedural planning and enabling same-day discharge strategies in select cases.

Standardized multidetector computed tomographic acquisition protocols for evaluating the LAA have been established using a 2-phase scan approach and may vary according to the scanner system used.<sup>17</sup> The first phase consists of a prospective or retrospective electrocardiographically gated scan acquisition during systole (typically 30%-60% of the R-R interval) that provides high-resolution images for a detailed assessment of LAA morphology and size. This is followed by a delayed acquisition, performed 30 to 180 seconds later, to reliably exclude the presence of an LAA thrombus in patients who may have delayed opacification of the LAA. A meta-analysis of 19 studies showed that MDCT has a high negative predictive value (96%-100%) for detecting LAA thrombi. Delaying imaging by

$\geq 30$  seconds after the contrast bolus is administered is mandatory and improves the mean positive predictive value from 41% to 92% or greater.<sup>18</sup>

Several image processing workstations (Vitrea Workstation, Aquarius Workstation, Brilliance Workstation, and 3mensio software, among others) use MPR (a volume-rendering process used to produce 2D planes from 3D data sets) to reassemble and manually manipulate images of the LAA and surrounding structures. By rotating the axial view 30° right anterior and the sagittal view 10° cranial, an oblique angle is reached to view the LAA orifice en face. Here, the maximum LAA depth, ostial diameter, and landing zone diameter are measured ([Figure 7, A and B](#)).

The 3D data provided by multidetector computed tomographic images enable advanced applications in procedural planning. For example, advanced software applications can assist with planning the optimal transeptal puncture location and C-arm position ([Figure 7, C](#)) and display a virtual device in a 3D rendering ([Figure 7, D](#)). Multidetector cardiac computed tomographic data sets can also be used for 3D printing, generating models to visualize the LAAO implantation and transeptal puncture *in vitro*. Studies have demonstrated that 3D printing improves device size accuracy compared with CT and TEE alone and can identify optimal transeptal puncture locations.<sup>19-21</sup> Additionally, artificial intelligence-enabled MDCT anatomic analyses and computer simulations can improve outcomes. De Backer *et al.*<sup>22</sup> demonstrated that using MDCT with FEops HEARTguide simulation technology (FEops) significantly improved procedural efficiency over standard practices, reducing total procedure times ( $55.2 \pm 24.7$  vs  $45.1 \pm 18.3$  min,



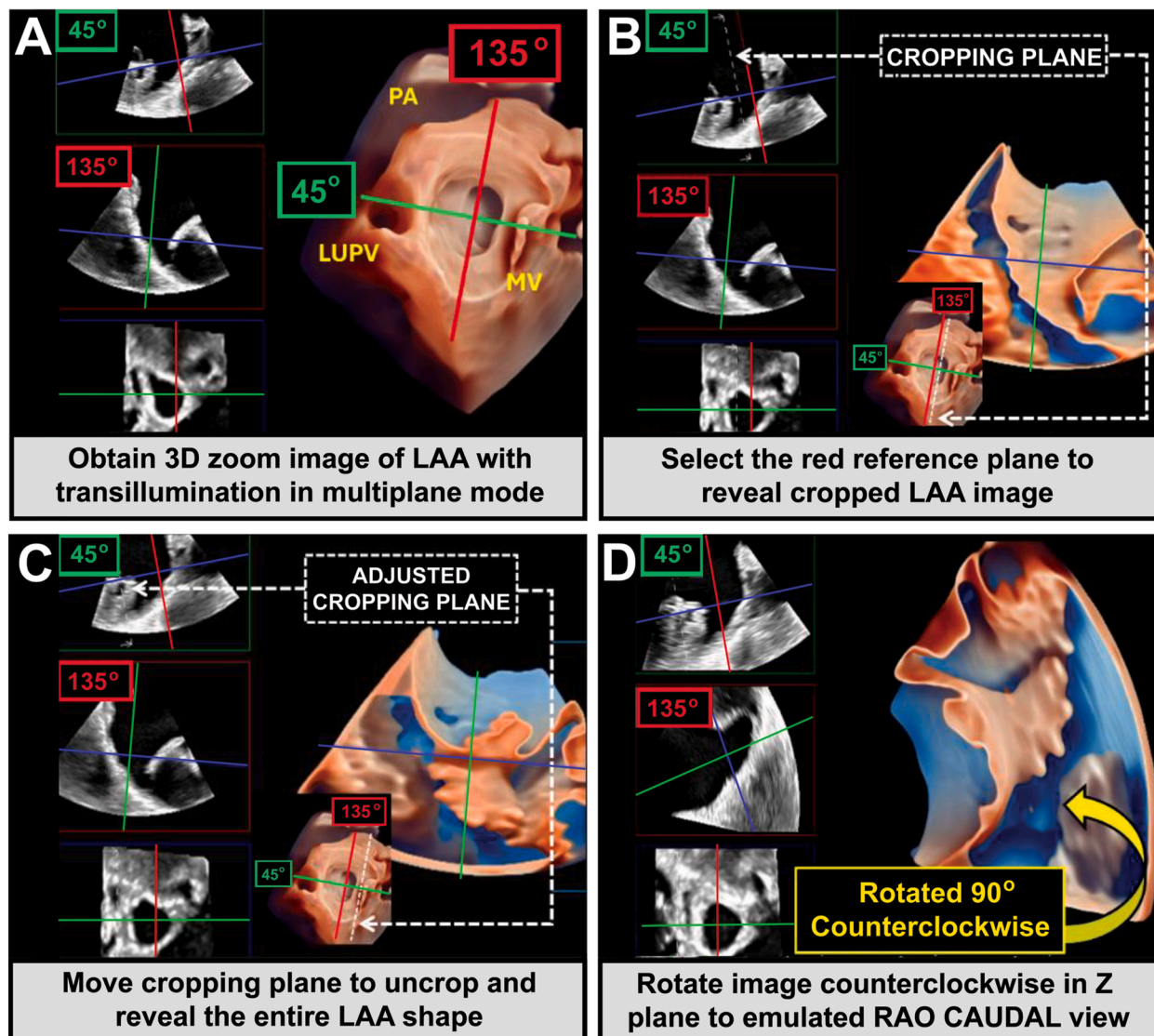


**Figure 3** LAA multiview maneuver to characterize LAA morphology by 3D TEE. **(A)** Obtain a 3D midesophageal LAA en face view at a 2D 45° angle (*green line*) with the transillumination feature activated. Establish an orthogonal plane (*red line*) using multiview. **(B)** Select the red reference plane and display the cropping plane (*dotted lines*). **(C)** Adjust the cropping plane leftward to reveal the full 3D anatomy of the LAA. **(D)** Rotate the 3D image 90° counterclockwise to simulate the standard fluoroscopic view used during percutaneous LAAO procedures. LUPV, Left upper pulmonary vein; MV, mitral valve; PA, pulmonary artery; RAO, right anterior oblique.

$P = .01$ ) and radiation times ( $17.6 \pm 11.4$  vs  $12.5 \pm 6.8$  min,  $P < .001$ ) and increasing rates of single-device, single-deployment (58.0% vs 29.9%,  $P < .001$ ).

### Comparison of Imaging Modalities

The first studies comparing imaging modalities for LAAO emerged in 2016. Wang *et al.*<sup>23</sup> ( $n = 53$ ) concluded that measurement by both 2D and 3D TEE significantly undersized the LAA landing zone ( $P \leq .0001$ ). Saw *et al.*<sup>24</sup> ( $n = 50$ ) highlighted that CT and TEE were not interchangeable, with MDCT measurements for both plug-like and disk-and-lobe devices being larger on CT than TEE. In one small study, the use of MDCT-derived LAA measurements significantly improved device size accuracy, achieving 92% accuracy (11

of 12) compared with 27% accuracy (three of 11) with TEE ( $P = .01$ ). This accuracy translated into enhanced procedural efficiency with reduced procedural time ( $55 \pm 17$  vs  $73 \pm 24$  min,  $P = .05$ ), fewer devices required per procedure ( $1.3 \pm 0.7$  vs  $2.5 \pm 1.2$  devices,  $P = .01$ ), and fewer delivery sheaths ( $1$  vs  $1.7 \pm 0.7$  sheaths per case,  $P = .01$ ) used.<sup>25</sup> A meta-analysis by Sattar *et al.*<sup>26</sup> demonstrated that despite LAA orifice measurements that were significantly larger on MDCT than on TEE, there was no significant difference in the number of devices used or in the odds of correct device sizing when only multidetector computed tomographic and transesophageal echocardiographic measurements were compared. However, when studies using MDCT-based 3D modeling were included, MDCT demonstrated significantly higher odds of correct device sizing compared with TEE (odds ratio, 1.64; 95% CI, 1.05-

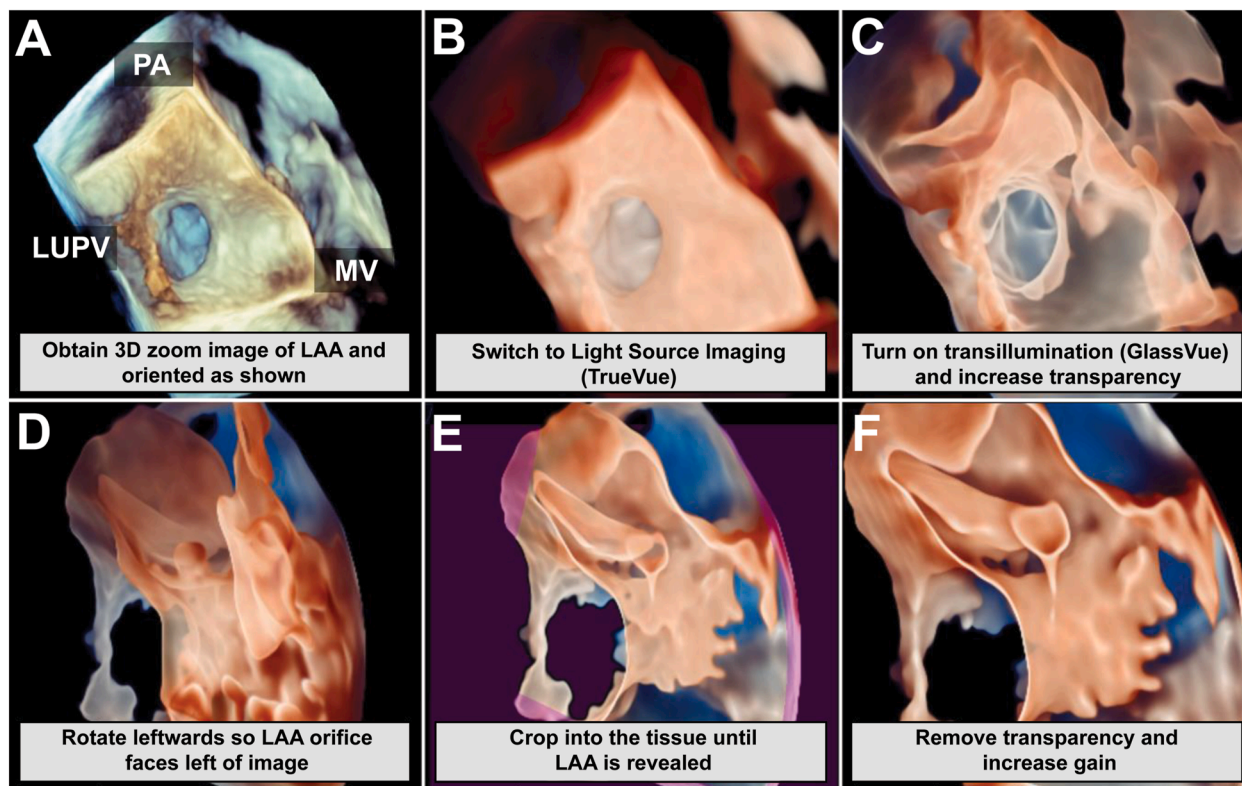


**Figure 4** Tilt-up-and-turn-left maneuvers to characterize LAA morphology by 3D TEE. **(A)** Display the standard en face view of the LAA orifice from the left atrial perspective. **(B)** Apply light-source manipulation to enhance visual details. **(C)** Use transillumination rendering of the LAA, increasing transparency to clearly demonstrate the orifice and outline the walls of the LAA body. **(D)** Rotate the image leftward along the vertical axis of the LAA to reveal the full body. **(E)** Selectively crop tissue to focus on specific areas. **(F)** Finalize the fully rendered LAA volume after decreasing transparency and increasing image gain. This orientation corresponds to the 2D transesophageal echocardiographic image at 135°. LUPV, Left upper pulmonary vein; MV, mitral valve; PA, pulmonary artery.

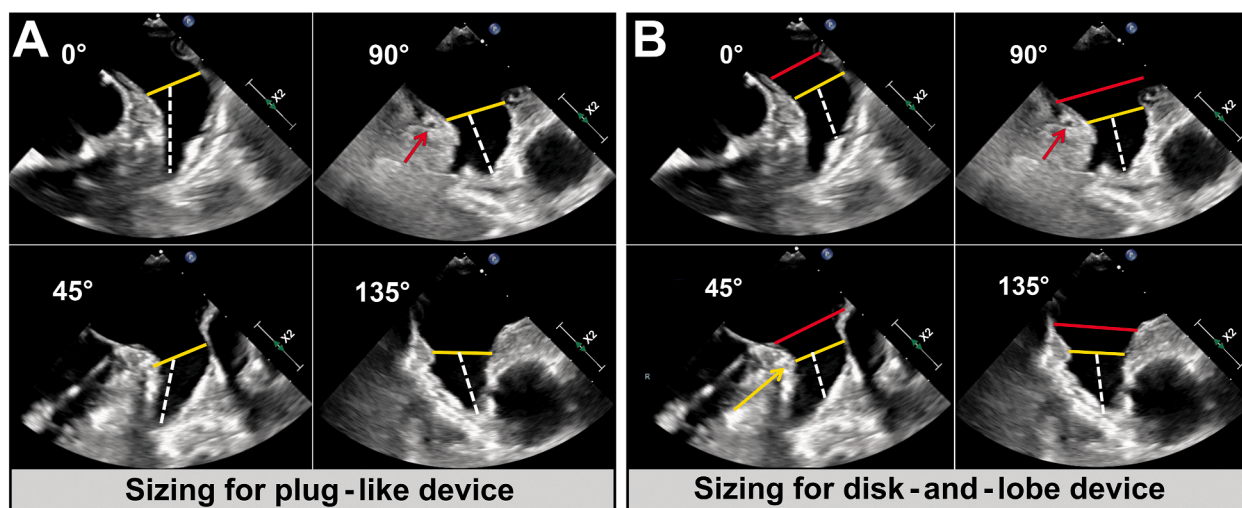


**Figure 5** LAA sizing for LAAO devices. **(A)** Two-dimensional TEE sizing for a pluglike occlusion device. The LAA landing zone diameters and depths are measured at four angles: 0°, 45°, 90°, and 135°. The LAA landing zone, which can be up to 2 cm below the left atrial ridge, is depicted by a *dotted white line* measured at the level of the circumflex artery (*red arrow*). **(B)** Two-dimensional TEE sizing for the disk-and-lobe device. The LAA landing zone diameters and depths are measured at four angles: 0°, 45°, 90°, and 135°. The LAA landing zone diameter is measured 10 to 12 mm from the anatomic orifice (*yellow arrow*), and the depth is measured from the ostium to the LAA wall in a plane perpendicular to the ostium. The *red arrow* indicates the circumflex artery.



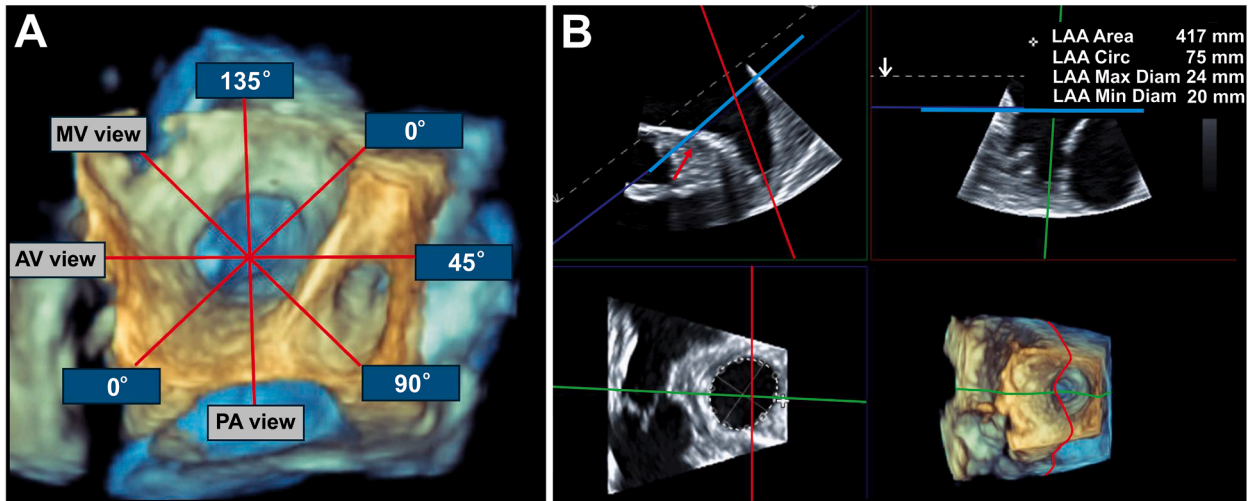


**Figure 6** Sizing of the LAA orifice using 3D transesophageal echocardiographic MPR. **(A)** Three-dimensional view of the LAA from the left atrium; the degrees shown correspond to 2D omniplane transesophageal echocardiographic views to assess the LAA. **(B)** A single-beat zoom capture acquires the entire LAA and surrounding structures. MPR is obtained. The *red and green planes* are locked and oriented toward the LAA apex, leaving the *blue plane* free for adjustment. The *blue plane* is oriented toward the plane of the LAA orifice, typically at the level of the left circumflex coronary artery (*red arrow*). The 3D Auto LAA feature (Philips) is used to obtain the maximum (Max) diameter (Diam) of the LAA orifice. AV, Aortic valve; Circ, circumference; Min, minimum; MV, mitral valve; PA, pulmonary artery.

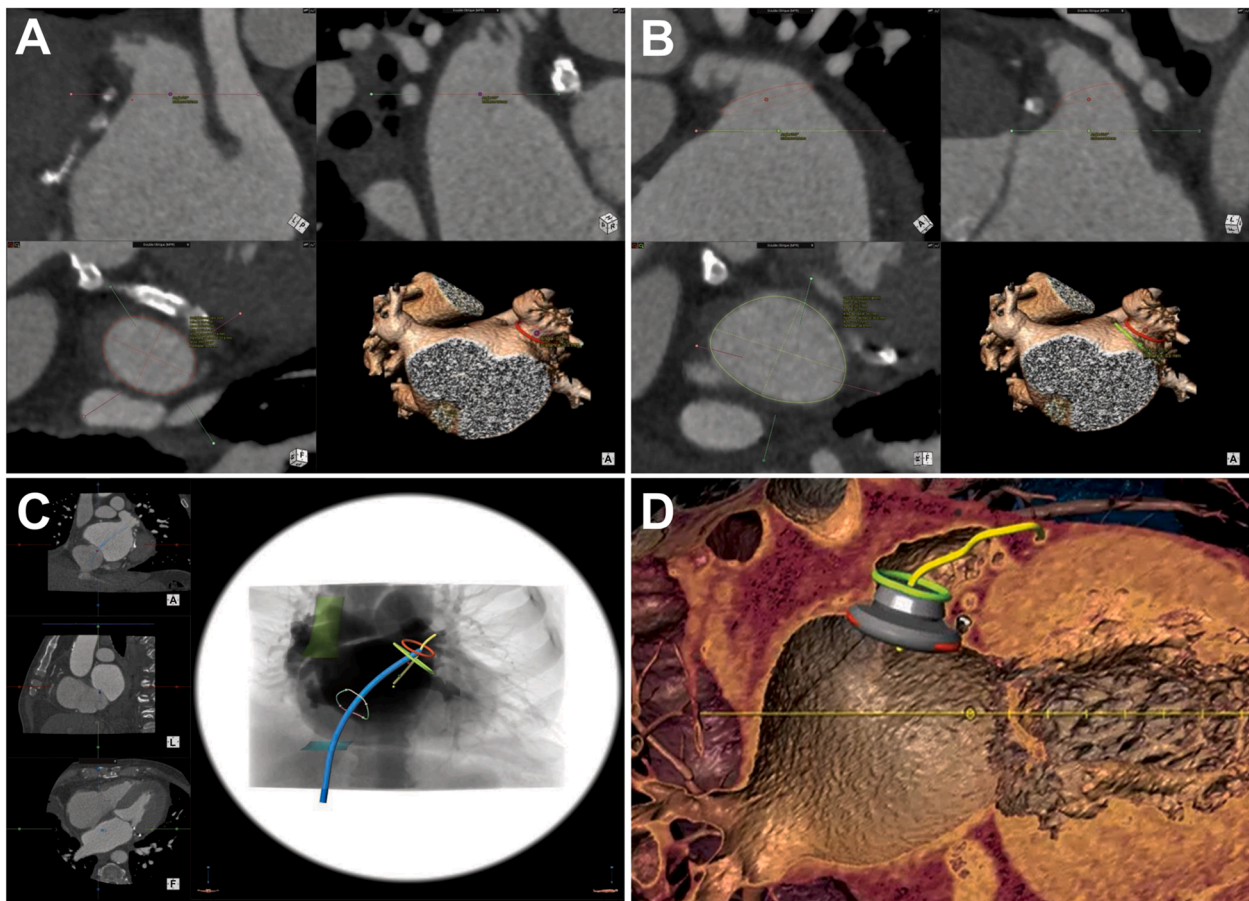


**Figure 7** Cardiac computed tomography for preprocedural planning for LAAO. In addition to excluding LAA thrombi, MDCT with 3D MPR can be used to perform precise measurements of the expected landing zone **(A)**, LAA orifice **(B)**, LAA depth, 3D morphology, and the relationship with the surrounding structures. Advanced software applications can also be of assistance in planning the optimal transseptal puncture location and C-arm position **(C)** and display a virtual device in the 3D rendering **(D)**.



**Table 1** Favorable and unfavorable anatomies for LAAO

Parameter	Favorable characteristics	Unfavorable characteristics
<b>Pluglike device</b>		
Landing zone	14–36 mm	>36 mm
Depth	~50% of device width	<50% of device width
Morphology	Windsock, cactus	Chicken wing, cauliflower/broccoli
Landing zone shape/eccentricity index	Round shape	Elliptical shape Eccentricity index $\geq 1.5$
Pectinates		Large midcavitary pectinates
<b>Disk-and-lobe device</b>		
Landing zone	11–31 mm	<11 mm or >31 mm
Depth	$\geq 10$ –12 mm	<10 mm
Morphology	Secondary lobes <1 cm from landing zone Chicken wing with short neck, acute bends	
Landing zone shape/eccentricity index	Oval landing zone	
Pectinates	Large midcavitary pectinates	

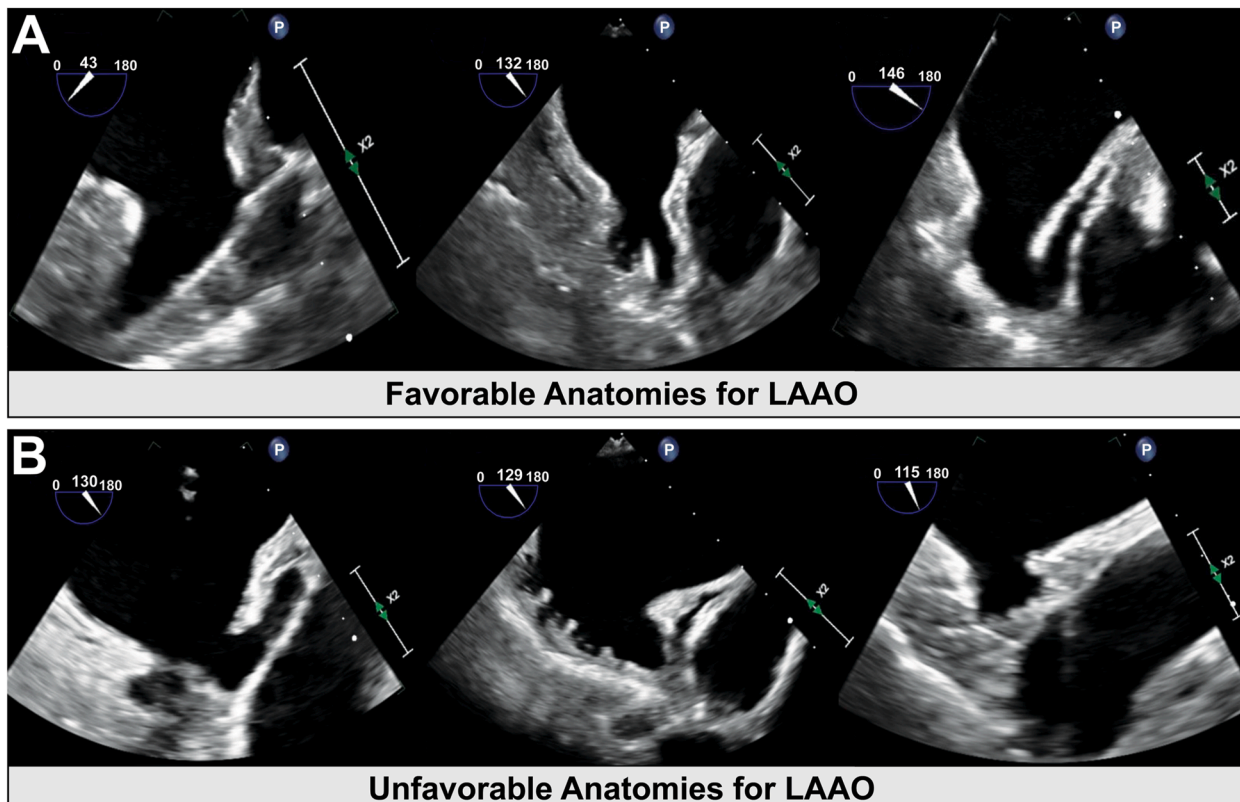


**Figure 8** Anatomic considerations for LAAO device selection. **(A)** Favorable morphologies for pluglike LAAO devices include windsock- and cactus-shaped LAAs, typically with orifice diameters ranging from 14 to 36 mm and depths approximately 50% of the intended device width. Favorable anatomies for disk-and-lobe devices include LAAs with orifice diameters of 11 to 31 mm and depths of  $\geq 10$  to 12 mm. **(B)** Unfavorable morphologies for pluglike devices include the chicken wing and cauliflower or broccoli shapes with shallow depths and orifice diameters <14 or >36 mm. Unfavorable conditions for disk-and-lobe devices include very small (<11 mm) or very large (>31 mm) landing zone diameters with insufficient depth (<10 mm).

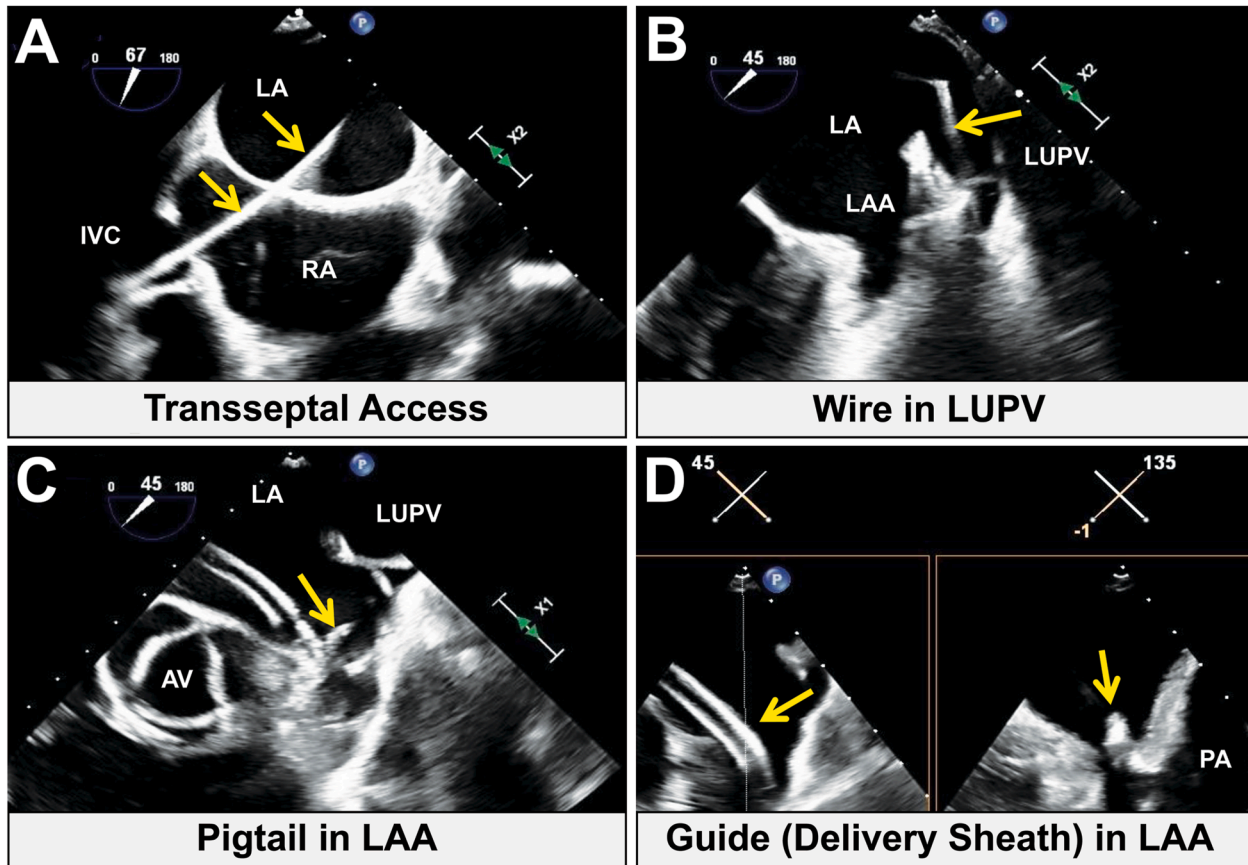


**Figure 9** Common steps for LAA closure procedure. **(A)** Transseptal access. Guided by TEE and fluoroscopy, transseptal access is usually achieved through an inferior and posterior approach. *Yellow arrows* demonstrate the sheath ([Video 1](#)). **(B)** Guidewire placement. The crossing sheath is exchanged with a guidewire (*yellow arrow*), which is placed in the left upper pulmonary vein (LUPV) ([Video 2](#)). **(C)** Delivery system advancement. A delivery system with a pigtail catheter (*yellow arrow*) is advanced into the left atrium (LA). Contrast angiography is performed to fluoroscopically evaluate the LAA ([Video 3](#)). **(D)** Catheter navigation. The guide catheter and pigtail combination is navigated to align the corresponding radiopaque marker band for the device size with the LAA ostium. Once the guide catheter (*yellow arrow*) is properly positioned, the pigtail is removed. *Yellow arrows* demonstrate the device and sheath ([Video 4](#)). AV, Aortic valve; IVC, inferior vena cava; PA, pulmonary artery; RA, right atrium.

2.56;  $P = .03$ ). Additionally, MDCT resulted in significantly reduced fluoroscopy time compared with TEE. These findings underscore the utility of preprocedural MDCT in improving procedural efficiency and outcomes in LAAO procedures.

#### Favorable and Unfavorable Anatomies for LAAO

The success of LAAO procedures depends on the anatomic characteristics of the LAA, which must be evaluated to select the appropriate device and optimize outcomes. Favorable and unfavorable morphologies can be described for pluglike devices and disk-and-lobe devices ([Table 1](#)).

**Pluglike Devices.** *Favorable Anatomies*—Windsock- and cactus-shaped LAAs that have an orifice measuring 14 to 36 mm and a minimum depth of approximately 50% of the device width allow higher compression and better success rates ([Figure 8, A](#)).

*Unfavorable Anatomies*—The chicken wing and cauliflower or broccoli morphologies, or orifices  $<14$  or  $>36$  mm, pose challenges with lower compression and success rates. Additionally, extremely elliptical LAA orifices and a high eccentricity index (maximum diam-

eter/minimum diameter  $\geq 1.5$ ) pose significant challenges, increasing the risk for residual leaks even with oversized devices. Insufficient depth ( $<50\%$  of device length) or large midcavitary pectinates may lead to a large shoulder with incomplete sealing, residual leaks, or device embolization ([Figure 8, B](#)).<sup>27</sup>

**Disk-and-Lobe Devices.** *Favorable Anatomies*—These devices perform well in LAAs with orifice diameters of 11 to 31 mm and depths of  $\geq 10$  to 12 mm. They are ideal for anatomies with oval-shaped landing zones, large midcavitary pectinates, and secondary lobes ( $<1$ -cm depth). Disk-and-lobe devices are positioned more proximally than pluglike devices, allowing adequate LAA closure in these anatomies. For LAAs that have a very short neck and sharp acute bends, such as in the chicken wing morphology, the implantation and complete closure rates are very high (98%-99%) because of the dual-closure design and ability to anchor on the proximal part of the LAA.<sup>28</sup>

*Unfavorable Anatomies*—Very small ( $<11$  mm) or very large ( $>31$  mm) landing zone diameters and insufficient depth ( $<10$  mm) compromise device stability and sealing.

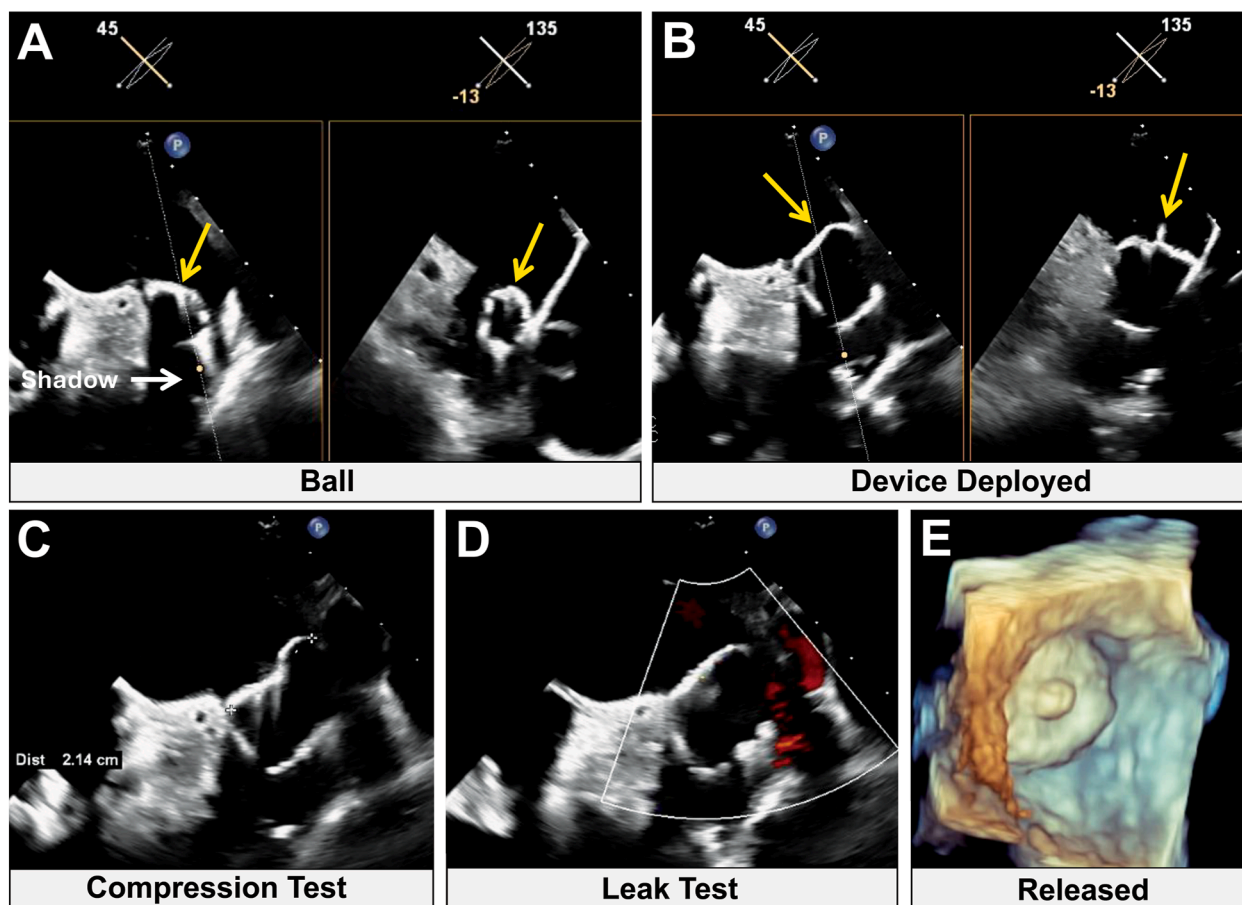


**Figure 10** Pluglike device procedure with TEE. **(A)** The delivery system (*yellow arrow, left*) is advanced until the distal marker bands of the delivery system and access sheath are aligned. The device is then unsheathed slowly until a ball shape (*yellow arrow, right*) is visualized (*Video 5*). **(B)** The device (*yellow arrows*) is fully unsheathed, and its position is evaluated using fluoroscopy and TEE (*Video 6*). **(C-E)** A prerelease evaluation is conducted using the “PASS” criteria (position: ensure that the plane of maximum diameter of the device is at or distal to the LAA ostium; anchor: test stability by retracting the deployment knob and letting go, assessing whether the device returns to its original position; size: confirm that the device shoulder is compressed to 10%-30% of its original size; seal: use TEE to assess for any residual flow, which must be <5 mm before release) (*Video 7*). Once all PASS criteria are met, the device may be released to deploy (*Video 8*).

Accurate preprocedural imaging and detailed anatomic assessment are essential for choosing the most suitable device, enhancing procedural success, and optimizing long-term patient outcomes.

## INTRAPROCEDURAL EVALUATION

### TEE

Intraprocedural TEE is the primary imaging modality for LAAO and was used in all the LAAO clinical trials. Intraprocedural TEE is performed to confirm LAA measurements and to rule out LAA thrombi. When spontaneous echocardiographic contrast (SEC) or sludge is present in the left atrium or LAA, differentiating a thrombus from the sludge or SEC becomes challenging, necessitating additional transesophageal echocardiographic enhancements.<sup>29</sup> Guidelines from the American Society of Echocardiography recommend the consideration of ultrasound enhancing agents during TEE for the assessment of LAA thrombus when there is SEC or poor visualization (Class 2a, Level of Evidence: B-NR).<sup>30</sup> Ultrasound enhancing agents

improve thrombus identification and differentiation of SEC degrees, with studies demonstrating increased interpretative confidence, reader agreement, and prevention of procedure cancellations.<sup>31</sup> Dobutamine and isoproterenol, both positive inotropic agents, have been shown to resolve LAA SEC and significantly increase peak LAA velocity.<sup>32,33</sup> There were no strokes, systemic embolisms, or device-related thrombi (DRTs) reported on follow-up with the use of dobutamine or isoproterenol.<sup>34</sup>

Disk-and-lobe and pluglike devices both require transfemoral venous access and have several common steps (*Figure 9, Videos 1-4*). Once femoral access is obtained, TEE is used to guide the transseptal puncture. A delivery catheter and needle are advanced to the interatrial septum. Both 2D or 3D transesophageal echocardiographic views can be used to visualize the inferior, superior, anterior, and posterior portions of the interatrial septum. The choice of transseptal puncture site is guided by the LAA's anatomy, with an inferoposterior puncture recommended in 75% to 80% of cases to ensure coaxial alignment between the delivery sheath and the proximal LAA central axis. However, an inferior but more central or anterior transseptal



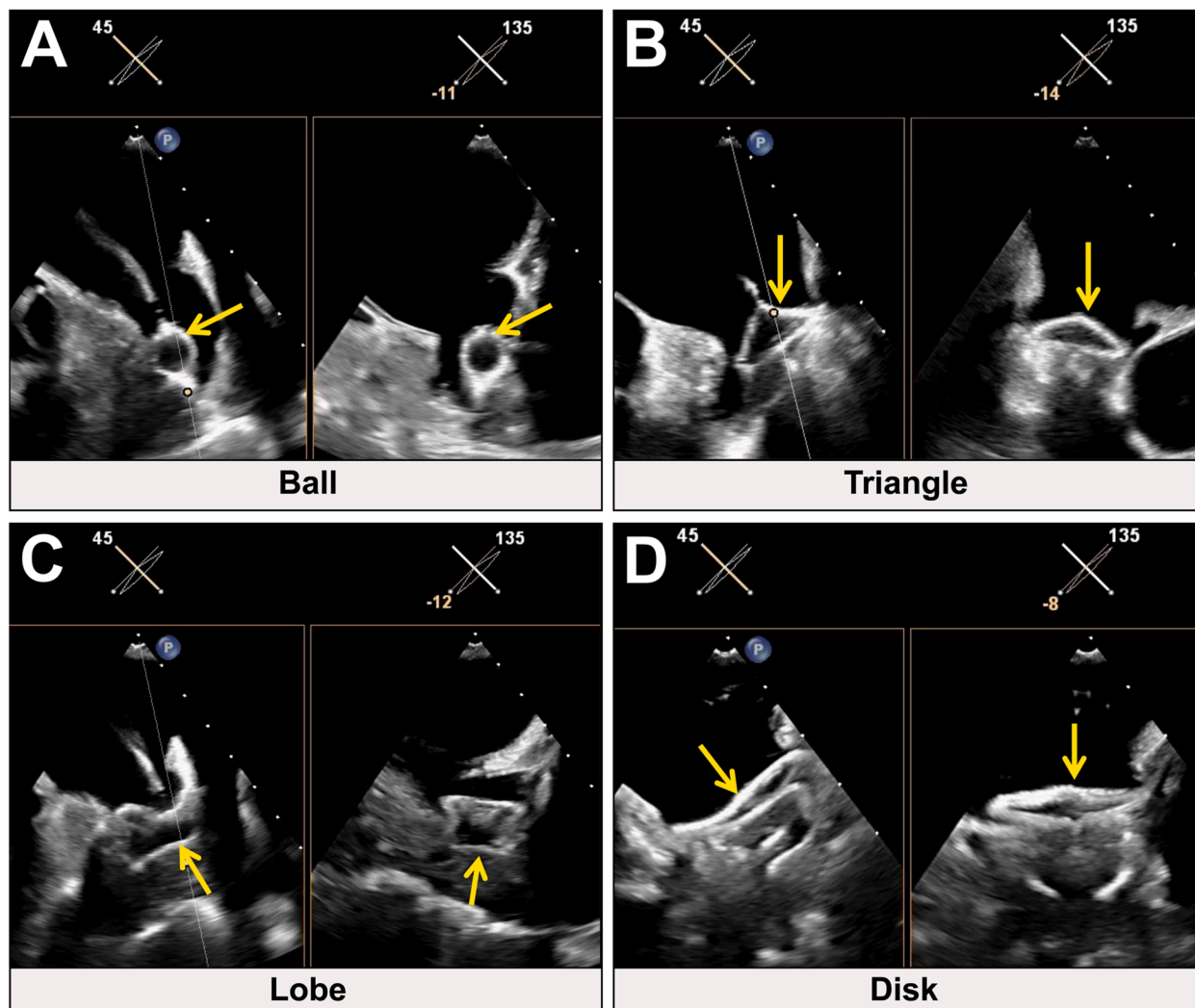


**Figure 11** Disk-and-lobe procedure steps with TEE. **(A)** The cable is advanced to push the device to the tip of the delivery sheath. Subsequently, the sheath is backed out until the device forms the “ball” (yellow arrow). It is essential to verify that the ball is coaxial to the neck of the LAA (Videos 9 and 10). **(B)** The cable is advanced slowly to form the “triangle” shape (yellow arrow; Video 11). **(C)** The delivery cable is advanced further to complete the deployment of the device lobe (yellow arrow; Video 12). **(D)** Deployment of the device disk (yellow arrow) is completed by advancing the delivery cable while simultaneously unsheathing the device disk (Video 13).

puncture is preferred in 20% to 25% of cases, particularly in those with reverse chicken wing LAA morphology or posterior bending of the proximal LAA.<sup>35,36</sup> As most LAAs are anteriorly directed, a posterior puncture is desirable in most cases. The 90° transesophageal view aids in gauging LAA direction, complemented by preprocedural cardiac computed tomographic analysis. Once the delivery sheath has crossed the interatrial septum, it is advanced into the left atrium and the distal end of the sheath is positioned near the LAA ostium.

The pluglike device is initially unsheathed to form a ball, which can be manipulated in the LAA to achieve an ideal trajectory and then be fully deployed. Figure 10 and Videos 5 to 8 outline the steps for deployment of a pluglike device. The location of the circumflex artery in relation to the ostium should be noted, with the plane of maximal device diameter positioned at or just distal to the ostium, ensuring that

any protrusion or “shoulder” (if present) does not exceed 40% to 50% of the device depth. For pluglike devices, the anatomic orifice is defined by a line connecting the circumflex artery and a point 10 to 20 mm inside the LAA from the left upper pulmonary vein ridge, described as the beginning of the trabeculated LAA, and is intended to be covered by the device. Compression is measured from shoulder to shoulder with the central metallic “threaded insert” visible on the left atrial side and is assessed at 0°, 45°, 90°, and 135°. A “tug test” is performed under transesophageal echocardiographic and/or fluoroscopic visualization to confirm stability, ensuring that the device returns to its original position. Once stability is confirmed, peridevice leaks (PDLs) should be carefully assessed using multiplanar imaging at 0°, 45°, 90°, and 135° with color Doppler and the Nyquist limit set at 20 to 30 cm/sec to detect low-velocity flows. Any significant

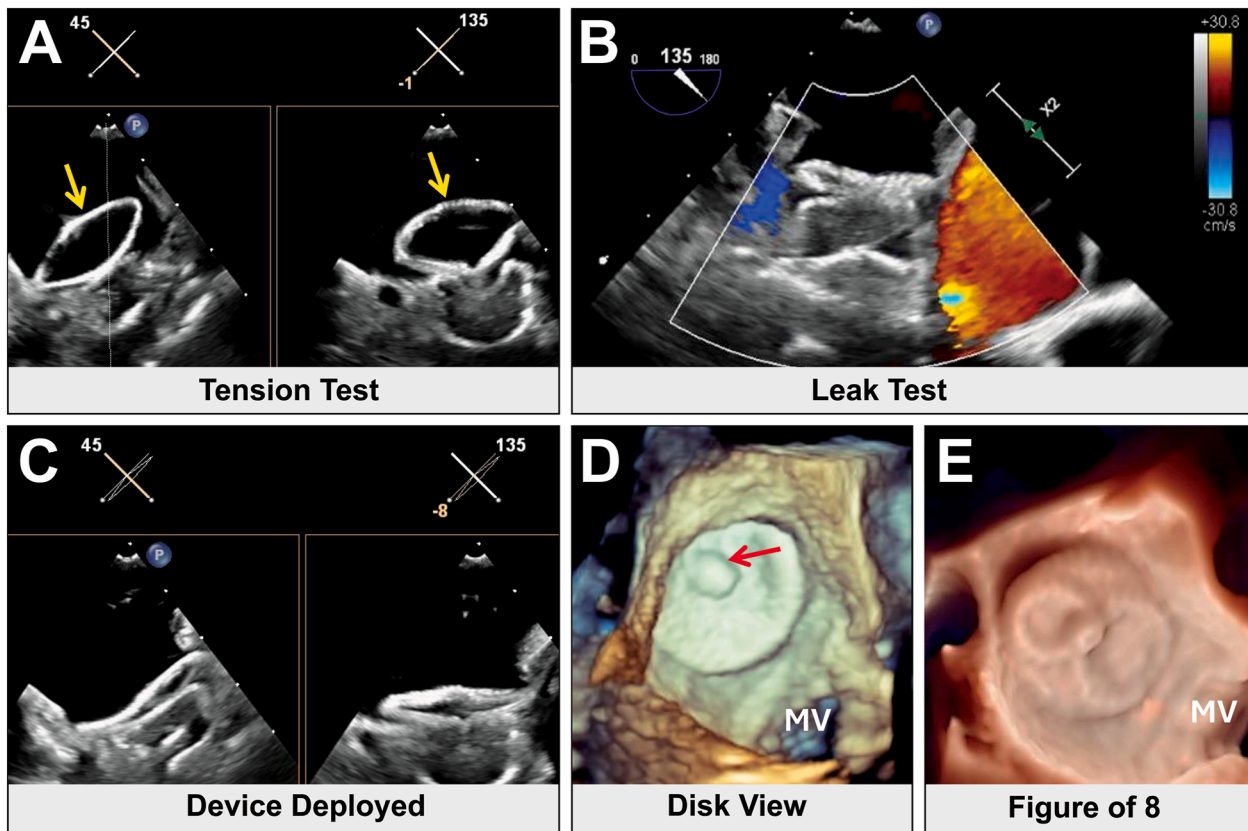


**Figure 12** Disk-and-lobe deployment steps with TEE. **(A)** Once the disk is deployed, a tension test is conducted to ensure that the lobe position remains unchanged (Video 14). The yellow arrows point to the football shape of the disk. **(B)** Residual flow around the device is assessed using TEE (Video 15). **(C)** After checking for any leaks and verifying a suitable position for release, the “CLOSE” criteria are reevaluated before the device is released (Video 16). **(D)** Following deployment, the device is visualized on conventional 3D TEE (Video 17). The red arrow indicates the proximal end screw. **(E)** 3D en face view of the disk-and-lobe occluder device, using light-source manipulation to depict a figure-of-8 configuration. Yellow arrows demonstrate the device and sheath.

PDL should be avoided, and the device recaptured and redeployed if needed.

For disk-and-lobe devices, the steps for deployment are outlined in Figures 11 and 12 (Videos 9-17). The device lobe should be two-thirds deeper than the circumflex artery to ensure proper sealing and compression. The lobe is initially unsheathed to form a ball. This ball can be manipulated into the LAA. Once the position and trajectory are optimized, this lobe is fully deployed, initially appearing as a triangle shape before full deployment. The disk is deployed subsequently, ensuring that it covers the anatomic ostium of the LAA and does not impinge upon the left superior pulmonary vein, which is separated from the LAA by a ridge.

Once the device is deployed, each type of device has a protocol for the assessment of position, stability, compression, and seal (Figure 13 for pluglike device, Figure 14 for disk-and-lobe device). A color Doppler “twinkling” artifact might be noted over the proximal surface of Nitinol-based polytetrafluoroethylene-covered devices. This artifact arises from ultrasound interactions with the strongly reflective surface and appears as a red-blue shimmer, mimicking flow, and should not be misinterpreted as PDL. This can be distinguished by its diffuse pattern, a lack of continuity across the device, and the absence of a corresponding signal on spectral Doppler. If the release

criteria are met, the device is released and the guide catheter is withdrawn from the left atrium; color Doppler and 2D TEE are then used to assess the size of the atrial septal defect and flow direction. A 3D view of the LAAO device is obtained to confirm its proximity to the mitral annulus and surrounding structures. A final assessment of pericardial effusion is performed before removing the transesophageal echocardiographic transducer.

### Micro- and Mini-TEE

Micro- and mini-transesophageal echocardiography probes, originally designed for pediatric diagnostic imaging, are emerging as alternatives to standard TEE probes for LAAO guidance, particularly in frail patients or those for whom general anesthesia is unsuitable. These smaller diameter probes (with 32 and 48 imaging elements, respectively, vs >2,500 in standard TEE) enable the use of conscious sedation, thereby reducing anesthesia-related risks and logistical challenges. In a recent study, micro- and mini-TEE provided adequate imaging in 99.3% of LAAO cases, with only 0.7% of cases requiring conversion to standard TEE, supporting the feasibility of these probes for this procedure.<sup>37</sup> However, limitations include reduced image quality as a result of fewer imaging

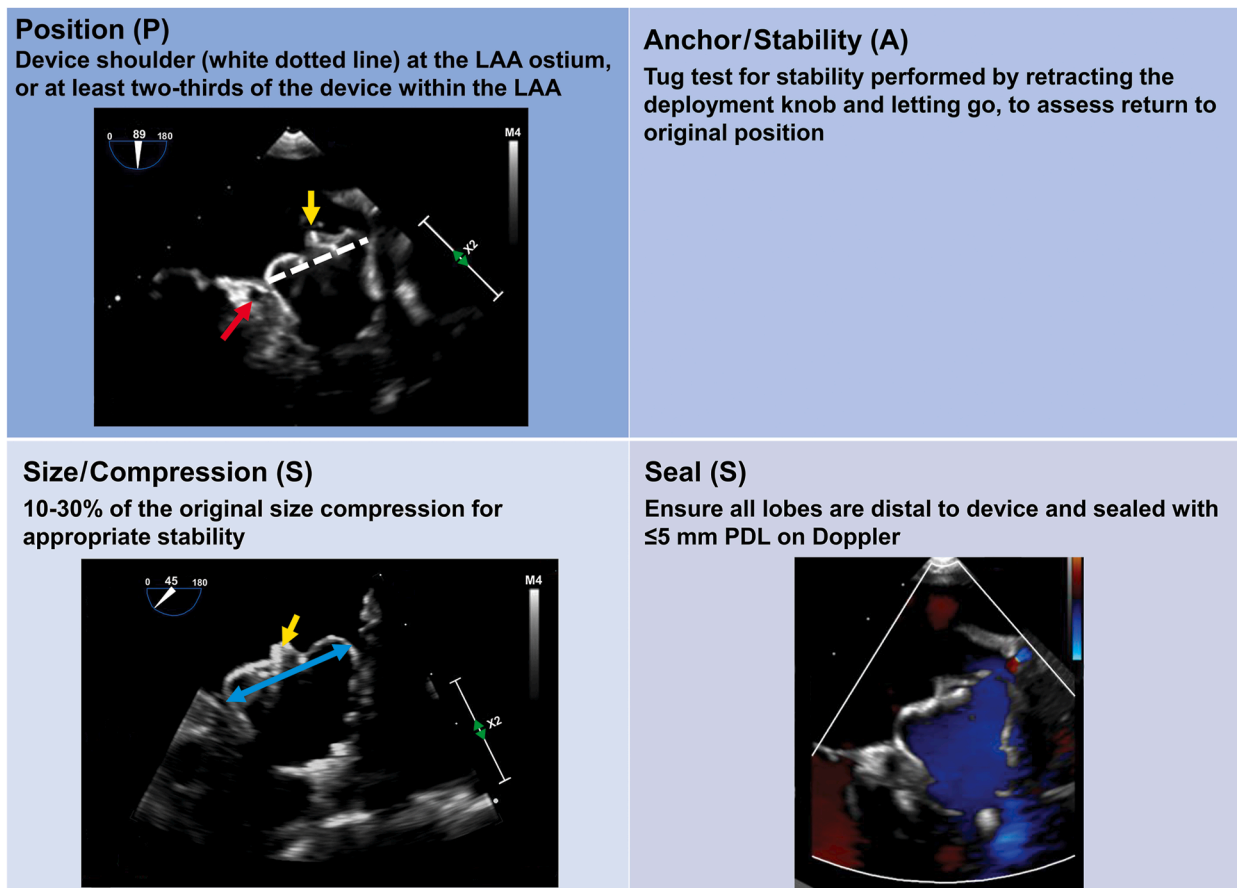


**Figure 13** Assessment of device release PASS criteria for pluglike device. The *yellow arrows* indicate the threaded insert, the *red arrow* indicates the left circumflex artery, and the *blue double-headed arrow* indicates compression of 15%.

elements, challenges in maintaining esophageal wall contact because of their smaller flexible design, and diminished far-field resolution in patients with large atria owing to higher probe frequencies. Despite these challenges, micro- and mini-TEE are particularly appealing to operators who seek minimalist LAAO approaches, offering a balance between TEE's familiarity and ICE's reduced anesthesia requirements, with the added benefit of lower gastrointestinal complication risk compared with standard TEE.

## ICE

ICE has gained popularity in guiding LAAO procedures, particularly with the advent of 3D real-time ICE. The procedure follows the same steps as with TEE. The intracardiac echocardiographic transducer is inserted into the right atrium and used to cross the interatrial septum. Imaging in three dimensions is essential to evaluate anterior-posterior and superior-inferior portions of the septum. Once the septum has been crossed, the intracardiac echocardiographic transducer is advanced through the puncture site into the left atrium. With the transducer in the left atrium, the absence of any LAA thrombi is confirmed and measurements of the LAA ostium and depth are obtained, preferably from the 3D data set. Intracardiac echocardiographic views should be opti-

mized to create three “TEE-like” views (Figure 15) to optimize the position and trajectory of the device. The mid left atrial view resembles the 45° transesophageal view and is used during LAA device deployment. The left superior pulmonary vein view resembles the 90° transesophageal view and is used to assess maximum LAA depth. The supramitral view is akin to the 135° (high-angle) transesophageal view, which is critical to assess device position, seal, and compression (Figure 15).

At present, it is unclear whether ICE-guided LAAO is a more cost-efficient method for LAA procedures and whether it is associated with better outcomes and shorter procedure times. In some cases, ICE could potentially eliminate the need for general anesthesia.<sup>38</sup> In a study by Berti *et al*,<sup>39</sup> ICE-guided LAAO had a procedural success rate of 93% and there was a significant correlation in measurements for device sizing between ICE and angiography. A recent meta-analysis demonstrated that ICE provides comparable efficacy and safety, with reduced use of contrast and shortened fluoroscopy and procedure times.<sup>40</sup> However, a multicenter study showed that although ICE-guided LAAO achieved high procedural success rates, TEE-guided procedures were associated with shorter procedure and fluoroscopy times.<sup>41</sup> The potential for ICE-guided LAAO without fluoroscopy is a significant advancement, with studies demonstrating feasibility for sizing, deployment, and PDL assessment without contrast. Successful cases with



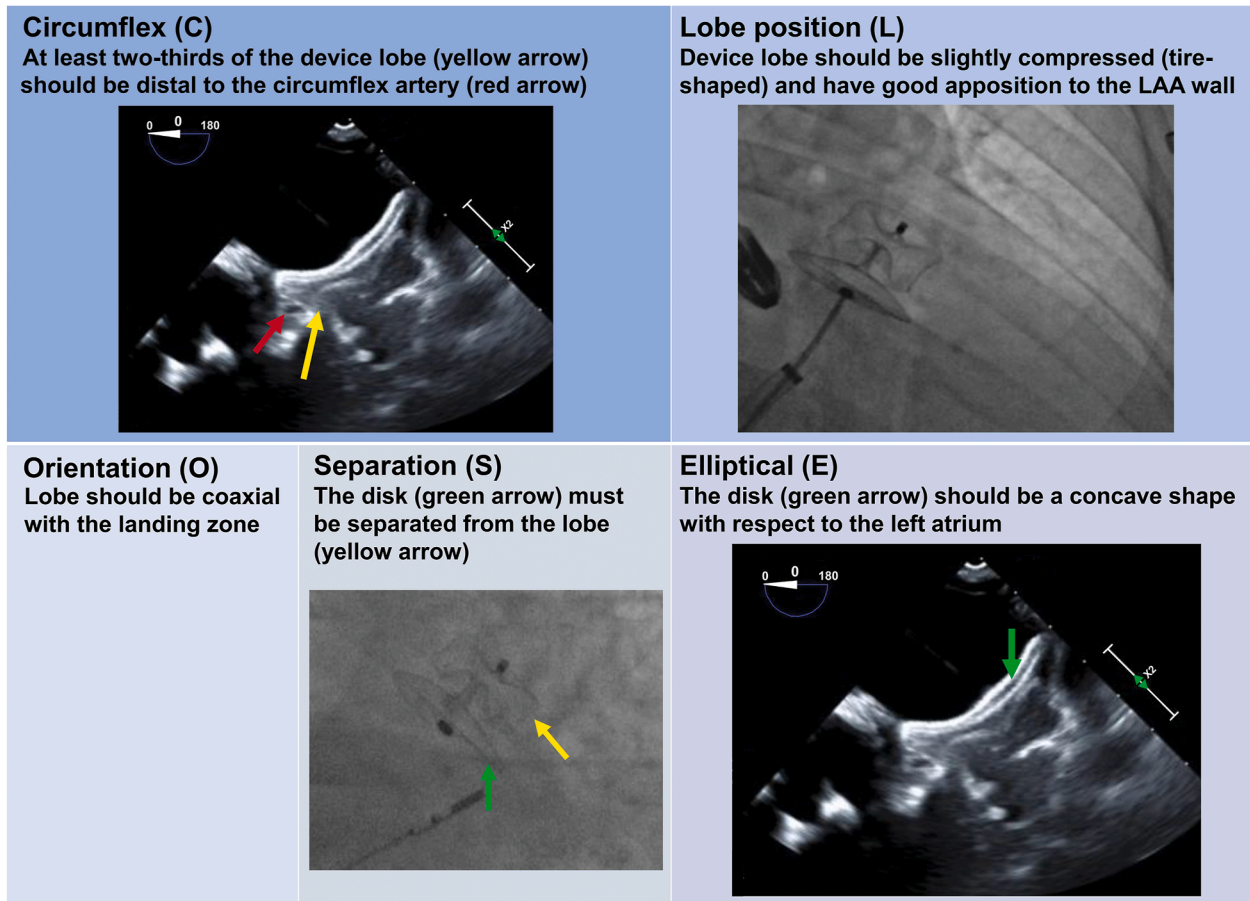


**Figure 14** Assessment of device release CLOSE criteria for disk-and-lobe device. The *red arrow* indicates the left circumflex artery. The *yellow arrows* indicate the lobe component of the device. The *green arrows* indicate the disk component of the device.

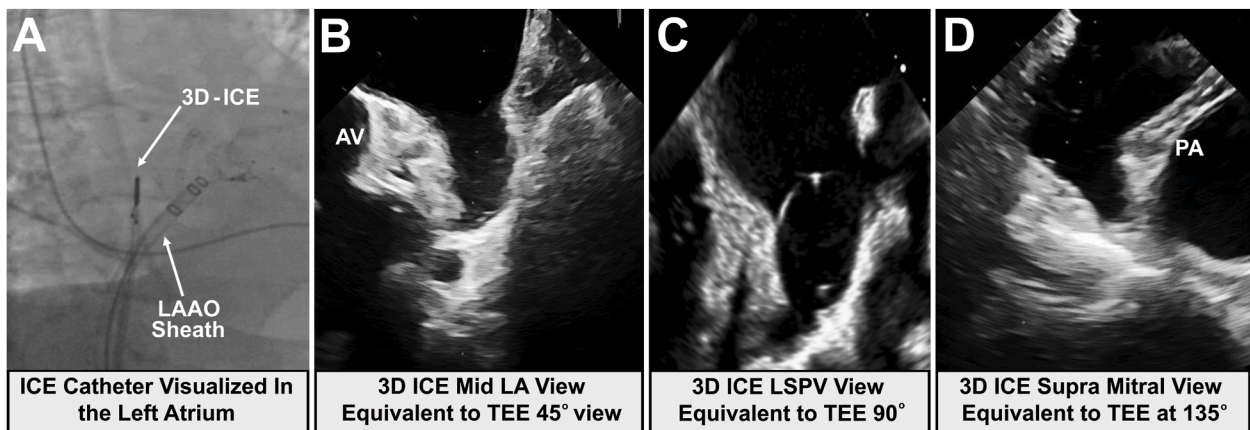


**Figure 15** Standard ICE views for LAAO. **(A)** The intracardiac echocardiography catheter is visualized in the left atrium on fluoroscopy. The three key intracardiac echocardiography probe positions commonly used to visualize the LAA during LAAO are the **(B)** mid left atrial (LA) view (equivalent to the transesophageal 45° view), the **(C)** left superior pulmonary vein view (equivalent to the transesophageal 90° view), and the **(D)** supramitral view (equivalent to the transesophageal 135° view). AV, Aortic valve; LSPV, left superior pulmonary vein; PA, pulmonary artery.

**Table 2** Complications of LAA procedures<sup>7,10,46-48</sup>

Complications	Percentage
Serious pericardial effusion	1.2–4.8
Major bleeding	0.6–1.3
Ischemic stroke	0.2–0.7
Device embolization	0.1–0.6
Procedure-related death	<0.5
Total major safety events	3.2–8.7

pluglike devices achieved zero fluoroscopy, with procedural times comparable with the conventional method.<sup>42,43</sup> This approach reduces radiation risks and eliminates the need for general anesthesia, enhancing patient comfort, although it involves a larger transeptal puncture and a learning curve. Furthermore, each modality comes with unique complications: whereas TEE has been associated with higher rates of gastrointestinal complications, ICE has been associated with increased rates of peripheral vascular and renal complications.<sup>44</sup> Additional considerations include the cost of the intracardiac echocardiographic catheter, the learning curve for operators, and current reimbursement challenges.

### Complications of LAAO Procedures

Intraprocedural complication rates are low with both types of devices. Pericardial effusion/tamponade can be a complication of transeptal puncture. Other complications include device-related embolization and procedure-related ischemic stroke.<sup>10</sup> The disk-and-lobe device has been found to have a slightly higher risk for pericardial tamponade or major bleeding.<sup>45</sup> Table 2 details the complications of LAAO procedures.<sup>7,10,46-48</sup> Importantly, the rate of complications decreases with operator experience. Intraprocedural imaging with TEE or ICE is key for both device placement and the monitoring of these complications.

## POSTPROCEDURAL EVALUATION

### Postprocedural Imaging Protocols

The 2023 consensus statement by the Society for Cardiovascular Angiography and Interventions and the Heart Rhythm Society recommends follow-up imaging with TEE or MDCT 45 to 90 days after LAAO to assess device sealing. A second follow-up at 1 year should be considered if there is concern about DRT or PDL. If DRT is detected, repeat imaging using TEE or MDCT every 45 to 90 days is recommended.<sup>36</sup>

Nestelberger *et al.*<sup>49</sup> recommended similar surveillance strategies: TEE or MDCT 6 to 12 weeks after LAAO and another routine TEE or MDCT at 12 months if the patient is at high risk for DRT. A key difference from the 2023 consensus statement is their recommendation for routine transthoracic echocardiography at 12 months to assess atrial sizes, ventricular and valvular function, and potential late device embolization. They also favor MDCT for surveillance at 6 to 12 weeks because of its higher spatial resolution, sensitivity in the detection of PDL, and noninvasive and nonfasting nature. However, they acknowledged the radiation and subsequent risk

associated with CT and emphasized that TEE remains a valuable modality for LAAO follow-up imaging.

### Imaging of DRT

DRT is one of the more troublesome findings on follow-up imaging, with the reported incidence ranging from 1.7% to 7%.<sup>50,51</sup> DRTs vary widely in size,<sup>52</sup> and their clinical impact is worrisome (Table 3<sup>52-61</sup>). Few trials were reassuring,<sup>9,56</sup> and the majority of data point to a 3.5 to 4 times higher risk for ischemic events in patients with DRT than in those without DRT.<sup>53,54,57</sup> The timing of the occurrence of DRT is somewhat unpredictable: 58% of DRT cases were diagnosed after 3 months in a meta-analysis and 18% to 36% of DRT were seen after 6 months in large registry studies, well after the presumed device endothelialization period.<sup>52,53,57</sup>

Predicting the occurrence of DRT requires consideration of several clinical, imaging, and procedural risk factors. The most commonly cited clinical risk factors include advanced age,<sup>50,58</sup> prior embolic events,<sup>54,58</sup> higher CHA<sub>2</sub>DS<sub>2</sub>-VASc score,<sup>59</sup> and permanent AF.<sup>50,52</sup> Preimplantation imaging findings that are associated with subsequent DRT include larger LAA orifice width, larger left atrial size, lower left ventricular ejection fraction, lower peak emptying velocity, and SEC.<sup>54,57,60-62</sup> Interestingly, neither LAA morphology nor anticoagulation regimen predicted DRT occurrence.<sup>53,57</sup>

Deep implantation has emerged as the strongest procedural risk factor for DRT.<sup>57,59,63</sup> Similarly, one study correlated the uncovered area—defined as the triangular area between the tip of the ridge, the surface of the device, and the mitral annulus—with the risk for DRT.<sup>63</sup> This cul-de-sac between the exposed ridge and the face of the device has been termed a “neoappendage”<sup>63,64</sup> and has been shown to increase turbulence. Additionally, off-axis deployment and residual PDL have also been associated with DRT risk.<sup>57,65</sup> Finally, the literature suggests that DRT can also occur centrally, adherent to the central screw of the device (Figure 16).<sup>52,57</sup>

TEE has historically been the standard postdeployment surveillance imaging modality.<sup>66</sup> The expert consensus definition of DRT by TEE is an echo density that is not explained by artifact, not typical of healing, visible in multiple planes, in contact with the device, and independently mobile.<sup>67,68</sup> The rise in MDCT has yielded markedly high rates of hypoattenuated thickening (HAT), which resembles thrombus but has an uncertain clinical significance. Recent studies show HAT in a significant majority of cases, leading to classification of HAT into low grade (smooth, covering the entire device, and continuous with the left atrial wall) and high grade (not continuous with the left atrial wall, having irregular borders or being pedunculated).<sup>69,70</sup> High-grade HAT, which occurs far less commonly at 2.8% to 5%, is associated with an increased risk for stroke compared with low-grade HAT.<sup>69,71</sup>

### Imaging of PDL

PDL following LAAO presents a notable risk for thromboembolic complications (Table 4<sup>9,51,56,72-76</sup>). The characteristics of these leaks can vary significantly on the basis of the occlusion device used and the anatomic features of the LAA. With pluglike devices, PDL typically manifests as flow between the left atrium and the distal part of the LAA. With disk-and-lobe devices, PDL may occur between the left atrium and the space between the disk and the lobe or beyond the lobe itself.

**Table 3** Summary of studies reporting DRT incidence, imaging modalities, and association with ischemic events

Study	DRT incidence	Patient factors	Procedural factors	Outcomes
Meta-analysis Alkhouli <i>et al.</i> <sup>53</sup>	<ul style="list-style-type: none"> <li>3.8% (pooled incidence)</li> <li>Following LAAO               <ul style="list-style-type: none"> <li>&lt;90 d: 42%</li> <li>90–365 d: 57%</li> <li>&gt;365 d: 1%</li> </ul> </li> <li>No difference in DRT incidence between devices</li> </ul>	<ul style="list-style-type: none"> <li>No specific consistent predictor was identified</li> </ul>	<ul style="list-style-type: none"> <li>No specific consistent predictor was identified</li> </ul>	Increase in ischemic events (13.5% vs 4.4%; OR, 4.15; 95% CI, 2.77–6.22; $P < .001$ ; $I^2 = 0$ )
PROTECT AF, PREVAIL, CAP, and CAP2 ad hoc analysis Dukkipati <i>et al.</i> <sup>54</sup>	<ul style="list-style-type: none"> <li>3.74%</li> <li>51% of DRT detected by scheduled TEE at 1 y</li> <li>62% detected during unscheduled TEE at 1 y</li> </ul>	<ul style="list-style-type: none"> <li>Permanent AF (OR, 2.24; 95% CI, 1.19–4.2; <math>P = .012</math>)</li> <li>History of TIA/stroke (OR, 2.31; 95% CI, 1.26–4.25; <math>P = .007</math>)</li> <li>Vascular disease (OR, 2.06; 95% CI, 1.08–3.91; <math>P = .028</math>)</li> </ul>	<ul style="list-style-type: none"> <li>LAA diameter (OR, 1.06; 95% CI, 1.01–1.12; <math>P = .019</math>)</li> <li>Lower LVEF (OR, 0.96 per 1% increase; 95% CI, 0.94–0.99; <math>P = .009</math>)</li> </ul>	Higher rates of ischemic stroke or systemic embolization (adjusted HR, 3.9; 95% CI, 2.3–6.8; $P < .001$ )
Amulet IDE Schmidt <i>et al.</i> <sup>55</sup>	<ul style="list-style-type: none"> <li>3.9% through 18 mo</li> <li>Amulet: 82% DRT <math>\leq</math>45 d</li> <li>Watchman: 73.8% DRT &gt;45 d</li> </ul>	<ul style="list-style-type: none"> <li>AF (HR, 2.44; 95% CI, 1.42–4.22; <math>P &lt; .01</math>)</li> <li>Female sex (HR, 1.65; 95% CI, 1.01–2.71; <math>P = .04</math>)</li> <li>Older age (HR, 1.04; 95% CI, 1.01–1.08; <math>P = .02</math>)</li> </ul>		No statistically significant associations between DRT and ischemic stroke or systemic embolization (3.1% vs 2.6% with vs without DRT), although numerically, there were more ischemic strokes and systemic embolisms after DRT compared with no DRT in the Watchman arm (5.5% vs 2.5%; HR, 2.15; 95% CI, 0.50–9.19)
EUROC-DRT registry Sedaghat <i>et al.</i> <sup>52</sup>	<ul style="list-style-type: none"> <li>Median of 93 d (IQR, 54–161 d)</li> <li>82% detected &lt;6 mo</li> <li>20% detected &gt;6 mo</li> </ul>		<ul style="list-style-type: none"> <li>Deep implantation</li> </ul>	Higher stroke rates in patients with residual DRT vs DRT resolution after 1 y (7.6% vs 6.5%; $P = .09$ ; mortality 15.0% vs 1.4%; $P = .01$ )
EWOLUTION registry Sedaghat <i>et al.</i> <sup>56</sup>	<ul style="list-style-type: none"> <li>4.1% by TEE or CT at a median of 54 d (IQR, 42–111 d)</li> <li>91.2% of DRT detected &lt;3 mo or at first TEE</li> </ul>	<ul style="list-style-type: none"> <li>Permanent AF (82.4% vs 64.9%; <math>P &lt; .01</math>)</li> <li>Dense SEC (26.5% vs 11.9%; <math>P = .03</math>)</li> </ul>	<ul style="list-style-type: none"> <li>LAA diameter (<math>22.8 \pm 3.5</math> vs <math>21.1 \pm 3.5</math> mm; <math>P &lt; .01</math>)</li> </ul>	No difference in rate of ischemic stroke/TIA (DRT 1.7% vs no-DRT 2.2% per year; $P = .80$ )
Global DRT registry Simard <i>et al.</i> <sup>57</sup>	<ul style="list-style-type: none"> <li>2.8%</li> <li><math>\leq</math>180 d: 64%</li> <li>&gt;180 d: 36%</li> </ul>	<ul style="list-style-type: none"> <li>Hypercoagulopathy (OR, 17.50; 95% CI, 3.39–90.45)</li> <li>Permanent AF (OR, 1.90; 95% CI, 1.22–2.97)</li> <li>Renal insufficiency (OR, 4.02; 95% CI, 1.22–13.25)</li> </ul>	<ul style="list-style-type: none"> <li>Pericardial effusion (OR, 13.45; 95% CI, 1.46–123.52)</li> <li>Deep implantation &gt;10 mm from limbus (OR, 2.41; 95% CI, 1.57–3.69)</li> </ul>	Increased rates of ischemic stroke in DRT vs no-DRT patients (16.9% vs 3.6%; $P = .0001$ )
Multicenter registry Fauchier <i>et al.</i> <sup>58</sup>	<ul style="list-style-type: none"> <li>7.2% per year</li> <li>8.3% with TEE and 5.3% with CT</li> <li>Mean time: <math>3.1 \pm 2.6</math> mo</li> </ul>	<ul style="list-style-type: none"> <li>Older age (HR, 1.07; 95% CI, 1.01–1.14; <math>P = .02</math>)</li> <li>Prior TIA/stroke (HR, 3.68; 95% CI, 1.17–11.62; <math>P = .03</math>)</li> </ul>	<ul style="list-style-type: none"> <li>No OAC (HR, 0.26; 95% CI, 0.09–0.77; <math>P = .02</math>)</li> <li>APT post-LAAO (HR, 0.10; 95% CI, 0.01–0.76; <math>P = .03</math>)</li> </ul>	Independent predictor of stroke and TIA (HR, 4.39; 95% CI, 1.05–18.43; $P = .04$ )
Single center Kaneko <i>et al.</i> <sup>59</sup>	<ul style="list-style-type: none"> <li>5% DRT</li> <li>5.1% at 45-d follow-up</li> </ul>	<ul style="list-style-type: none"> <li>Higher CHA<sub>2</sub>DS<sub>2</sub>-VASc score (OR, 2.8; 95% CI, 1.2–7; <math>P = .02</math>)</li> </ul>	<ul style="list-style-type: none"> <li>Deep device implantation (OR, 24.7; 95% CI, 1.3–458.2; <math>P = .03</math>)</li> </ul>	Not assessed

(Continued)



Table 3 (Continued)

Study	DRT incidence	Patient factors	Procedural factors	Outcomes
Prospective global Amulet registry Aminian <i>et al.</i> <sup>60</sup>	<ul style="list-style-type: none"> <li>• 1.7% per year</li> <li>• DRT scheduled follow-up TEE in 10 cases, unscheduled TEE seven cases, and CT one patient</li> </ul>	<ul style="list-style-type: none"> <li>• Larger LAA orifice width (HR, 1.09, 95% CI, 1–1.19; <math>P = .04</math>)</li> </ul>		Greater risk for ischemic stroke/TIA (HR, 5.27; 95% CI, 1.58–17.55; $P = .007$ )
EUROC-DRT registry Vij <i>et al.</i> <sup>61</sup>	<ul style="list-style-type: none"> <li>• 20% patients with DRT</li> <li>• TEE: 88.4% of cases detected</li> <li>• CT: 11.6% of cases detected</li> <li>• Mean of <math>147 \pm 219</math> d</li> </ul>	<ul style="list-style-type: none"> <li>• Age (OR, 1.16; 95% CI, 1.07–1.25; <math>P &lt; .01</math>)</li> <li>• Prior stroke/TIA (OR, 3.71; 95% CI, 1.19–11.56; <math>P = .02</math>)</li> <li>• SEC (OR, 5.08; 95% CI, 1.37–18.84; <math>P = .02</math>)</li> </ul>	<ul style="list-style-type: none"> <li>• Deep implantation predictive in univariate analysis after PSM</li> </ul>	Significant increased risk for stroke with DRT (13.55%) compared with no DRT (3.8%) within 2 y (HR, 4.21; 95% CI, 1.88–9.49; $P < .01$ )

APT, Antiplatelet; HR, hazard ratio; IQR, interquartile range; LVEF, left ventricular ejection fraction; OAC, oral anticoagulation; OR, odds ratio; PSM, propensity score matching; TIA, transient ischemic attack.

The mechanisms of leaks for pluglike devices include edge leak, uncovered lobe or proximal LAA, and fabric leak (Figure 17). For disk-and-lobe devices, leaks can occur between the disk and the lobe, into the distal LAA, because of uncovered proximal tissue, or from fabric leak.<sup>77</sup> The clinical implications of the different types of leaks with disk-and-lobe devices have not been adequately studied, highlighting the need for further research.

### Size of PDLs and Thromboembolic Risk

Traditionally a vena contracta of PDL edge leak of  $<5$  mm has been considered acceptable for the pluglike device; however, emerging data challenge this threshold.<sup>9,72,73,75</sup> Table 3 summarizes key studies showing the PDL incidence and its association with ischemic events. Alkhouli *et al.*<sup>72</sup> reported a 10% to 15% increase in the 1-year risk-adjusted rates of systemic thromboembolic events for patients with small leaks, with a hazard ratio of 1.152 (95% CI, 1.025–1.294), compared with patients without leaks. Large PDLs, though rare, have been associated with a significantly higher risk for thromboembolism when compared with patients with no PDL.<sup>75</sup> This underscores the

importance of accurate detection and ongoing surveillance of these leaks to manage and mitigate associated risks effectively.

### Imaging Modalities for Detecting PDL

Detecting and characterizing PDL is critical yet challenging because of varied detection methods and the lack of a standardized definition. TEE and MDCT are the primary imaging modalities used to assess PDL. In a study involving 346 patients who underwent both TEE and MDCT at 8 weeks after LAAO with a disk-and-lobe device, PDL was detected in 110 patients (32%) on TEE, whereas MDCT identified PDL in 210 patients (61%).<sup>78</sup> Another study also demonstrated that the incidence of PDL detected by MDCT was higher (52%) than observed with TEE (34.3%).<sup>79</sup> These studies indicate a substantially higher occurrence of PDL detection with MDCT compared with TEE, revealing a significant discrepancy in leak quantification between these modalities. However, no standardized sizing thresholds currently exist for MDCT, as initial trials were performed with TEE. This highlights an area in which further research is needed.

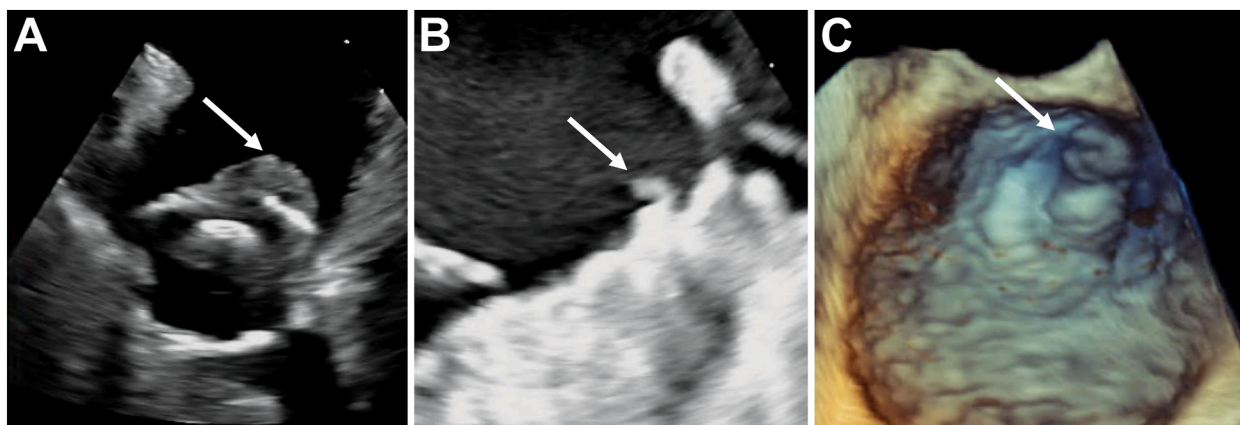
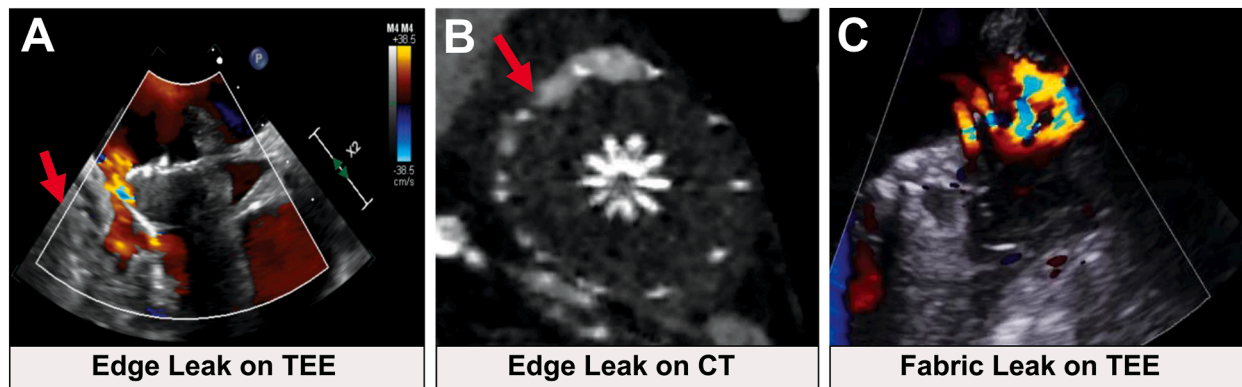


Figure 16 DRT. (A) A thrombus (arrow) on a deeply implanted device is seen on 2D TEE. (B) A thrombus (arrow) on the threaded insert of a device is seen on 2D TEE. (C) A DRT (arrow) in the neoappendage created between the device face and the left atrial pulmonary vein/LAA ridge is seen on 3D TEE.

**Table 4** Summary of studies reporting PDL incidence, imaging modalities, and association with ischemic events

Study	Device(s)	Study population	Imaging modality	PDL incidence	Association of PDL with ischemic events
NCDR LAAO registry <sup>72</sup>	Watchman 2.5	51,333	TEE (45 d)	<5 mm: 25.8% >5 mm: 0.7%	Small PDLs (1–5 mm): ↑ stroke/TIA/systemic embolization (aHR, 1.15; 95% CI, 1.02–1.29) compared with no PDL
PROTECT AF and PREVAIL +CAP2 <sup>73</sup>	Watchman 2.5	1,054	TEE (45 d, 12 mo)	≤3 mm: 24.2% 3–5 mm: 14.1% >5 mm: 1.5%	PDL ≤5 mm at 1 y was a significant predictor of ischemic stroke/systemic embolism (HR, 1.75; 95% CI, 1.06–2.89; <i>P</i> = .03)
AMULET IDE <sup>9</sup>	Amulet and Watchman 2.5	1,878	TEE (45 d, 12 mo)	At 45 days: • Amulet 0–3 mm: 27% >3–5 mm: 9% >5 mm: 1% • Watchman 0–3 mm: 29% 3–5 mm: 22% >5 mm: 3%	Not assessed
AMULET IDE subanalysis <sup>74</sup>	Amulet (801 patients) and Watchman 2.5 (792 patients)	1,593	TEE at 45 d, 12 mo	At 45 days: • Watchman 0–3 mm: 74.1% ≥3–5 mm: 25.9% >5 mm: 3.2% • Amulet 0–<3 mm: 88.8% ≥3–5 mm: 1.2% >5 mm: 1.1% • <i>P</i> < .01 for all At 12 months: • Watchman: residual PDL ≤5 mm: 97.2% ≥5 mm: 2.8% • Watchman: new PDL ≥3 mm: 8.3% • Amulet: residual PDL ≤5 mm: 99.4% >5 mm: 0.6% • Amulet: new PDL ≥ 3 mm: 4.2%	PDL ≥3 mm: higher 1-mo rates of ischemic stroke or systemic embolization compared with those with PDL <3 mm (3.6% vs 1.8%; unadjusted HR, 2.03; 95% CI, 0.96–4.29; <i>P</i> = .06)
Meta-analysis of residual leaks following LAAO <sup>75</sup>	Amulet and Watchman	61,666	TEE, CT	• TEE Any PDL: 26.5% >1 mm: 15% >3 mm: 9.6% >5 mm: 0.9% • CT PDL >0 mm: 57.3%	Any TEE-reported PDL was significantly associated with twofold increase odds of thromboembolism (pOR, 2.04, 95% CI, 1.52–2.74; <i>I</i> <sup>2</sup> = 28%) compared with no PDL
PINNACLE FLX <sup>51</sup>	Watchman FLX	400 patients	TEE (45 d, 6 mo, and 1 y)	17.2% at 45 d 10.5% at 6 mo (>0 and ≤5mm) No PDL >5 mm	Not assessed
EWOLUTION <sup>56</sup>	Watchman	835	TEE (45 d)	8.4% (any PDL)	Not assessed
Global Amulet study <sup>76</sup>	Amulet	1,088	TEE (45 d)	9.9% (any PDL)	Not assessed

aHR, Adjusted hazard ratio; HR, hazard ratio; OR, odds ratio; pOR, pooled odds ratio; TIA, transient ischemic attack.



**Figure 17** Mechanisms of residual leaks after LAAO with a pluglike occluder. **(A)** Edge leak seen on TEE. **(B)** Uncovered lobe seen on CT. **(C)** Fabric leak seen on TEE.

## CONCLUSIONS

Multimodality imaging is essential for optimizing outcomes in LAAO. Preprocedural evaluation using TEE and MDCT is essential for assessing LAA morphology and determining the appropriate device size. MDCT offers superior multiplanar and 3D imaging, whereas TEE provides functional insights that are vital for determining patient eligibility and selecting the optimal device for the procedure. Intraprocedural imaging with TEE or ICE ensures real-time guidance for accurate and efficient device placement. Postprocedural follow-up with TEE or MDCT is essential for monitoring device stability and assessing PDL and DRT (*Central Illustration*).

The selection of appropriate imaging modalities for percutaneous LAAO is crucial for ensuring optimal outcomes. The integration of multimodality imaging—leveraging the strengths of TEE, MDCT, and ICE—is essential for accurate device sizing, successful implantation, and timely detection of complications. As imaging technologies advance, these strategies will continue to evolve, further improving long-term outcomes for patients undergoing LAAO.

## CONFLICTS OF INTEREST

Dr Saric is a member of the speakers bureaus of Abbott, Boston Scientific, Medtronic, and Philips and the advisory board of Siemens. Dr Jain is a speaker and consultant for Medtronic, Philips, Edwards Lifesciences, and GE Healthcare and a member of the advisory boards of Medtronic and GE Healthcare.

## ACKNOWLEDGMENTS

We thank Jennifer Pfaff for editorial preparation of the manuscript and Brian Schurrer for assistance with the figures.

## SUPPLEMENTARY DATA

Supplementary data related to this article can be found at <https://doi.org/10.1016/j.echo.2025.07.009>.

## REFERENCES

- Jiao M, Liu C, Liu Y, et al. Estimates of the global, regional, and national burden of atrial fibrillation in older adults from 1990 to 2019: insights from the global burden of disease study 2019. *Front Public Health* 2023;11:1137230.
- Lin HJ, Wolf PA, Kelly-Hayes M, et al. Stroke severity in atrial fibrillation. The Framingham Study. *Stroke* 1996;27:1760-4.
- Blackshear JL, Odell JA. Appendage obliteration to reduce stroke in cardiac surgical patients with atrial fibrillation. *Ann Thorac Surg* 1996;61:755-9.
- Holmes DR Jr, Alkhouli M, Reddy V. Left atrial appendage occlusion for the unmet clinical needs of stroke prevention in nonvalvular atrial fibrillation. *Mayo Clin Proc* 2019;94:864-74.
- Madden JL. Resection of the left auricular appendix; a prophylaxis for recurrent arterial emboli. *J Am Med Assoc* 1949;140:769-72.
- Reddy VY, Sievert H, Halperin J, et al. Percutaneous left atrial appendage closure vs warfarin for atrial fibrillation: a randomized clinical trial. *JAMA* 2014;312:1988-98.
- Holmes DR Jr, Kar S, Price MJ, et al. Prospective randomized evaluation of the watchman left atrial appendage closure device in patients with atrial fibrillation versus long-term warfarin therapy: the PREVAIL trial. *J Am Coll Cardiol* 2014;64:1-12.
- Reddy VY, Doshi SK, Kar S, et al. 5-year outcomes after left atrial appendage closure: from the PREVAIL and PROTECT AF trials. *J Am Coll Cardiol* 2017;70:2964-75.
- Lakkireddy D, Thaler D, Ellis CR, et al. Amplatzer Amulet left atrial appendage occluder versus watchman device for stroke prophylaxis (Amulet IDE): a randomized, controlled trial. *Circulation* 2021;144:1543-52.
- Holmes DR, Reddy VY, Turi ZG, et al. Percutaneous closure of the left atrial appendage versus warfarin therapy for prevention of stroke in patients with atrial fibrillation: a randomised non-inferiority trial. *Lancet* 2009;374:534-42.
- Hahn RT, Saric M, Faletra FF, et al. Recommended standards for the performance of transesophageal echocardiographic screening for structural heart intervention: from the American Society of Echocardiography. *J Am Soc Echocardiogr* 2022;35:1-76.
- Hayes DE, Bamira D, Vainrib AF, et al. Left atrial appendage tilt-up-and-turn-left maneuver: a novel three-dimensional transesophageal echocardiography imaging maneuver to characterize the left atrial appendage and to improve transcatheter closure guidance. *CASE (Phila)* 2023;7:391-5.
- Vainrib A, Saric M. Quick three-dimensional transesophageal echocardiography of left atrial appendage (LAA) anatomy using the LAA multiview technique. *CASE (Phila)* 2023;7:461-2.
- Zhang L, Cong T, Liu A. Percutaneous closure of the left atrial appendage: the value of real time 3D transesophageal echocardiography and the



- intraoperative change in the size of the left atrial appendage. *Echocardiography* 2019;36:537-45.
15. Yosefy C, Laish-Farkash A, Azhibekov Y, et al. A new method for direct three-dimensional measurement of left atrial appendage dimensions during transesophageal echocardiography. *Echocardiography* 2016;33:69-76.
  16. Filby SJ, Dallan LAP, Cochet A, et al. Left atrial appendage occlusion using cardiac CT angiography and intracardiac echocardiography: a prospective, single-center study. *J Invasive Cardiol* 2021;33:E851-6.
  17. Korsholm K, Berti S, Iriart X, et al. Expert recommendations on cardiac computed tomography for planning transcatheter left atrial appendage occlusion. *JACC Cardiovasc Interv* 2020;13:277-92.
  18. Romero J, Husain SA, Kelesidis I, et al. Detection of left atrial appendage thrombus by cardiac computed tomography in patients with atrial fibrillation: a meta-analysis. *Circ Cardiovasc Imaging* 2013;6:185-94.
  19. Hell MM, Achenbach S, Yoo IS, et al. 3D printing for sizing left atrial appendage closure device: head-to-head comparison with computed tomography and transesophageal echocardiography. *EuroIntervention* 2017;13:1234-41.
  20. Obasare E, Mainigi SK, Morris DL, et al. CT based 3D printing is superior to transesophageal echocardiography for pre-procedure planning in left atrial appendage device closure. *Int J Cardiovasc Imaging* 2018;34:821-31.
  21. Hozman M, Herman D, Zemanek D, et al. Transseptal puncture in left atrial appendage closure guided by 3D printing and multiplanar CT reconstruction. *Catheter Cardiovasc Interv* 2023;102:1331-40.
  22. De Backer O, Iriart X, Kefer J, et al. Impact of computational modeling on transcatheter left atrial appendage closure efficiency and outcomes. *JACC Cardiovasc Interv* 2023;16:655-66.
  23. Wang DD, Eng M, Kupsky D, et al. Application of 3-dimensional computed tomographic image guidance to WATCHMAN implantation and impact on early operator learning curve: single-center experience. *JACC Cardiovasc Interv* 2016;9:2329-40.
  24. Saw J, Fahmy P, Spencer R, et al. Comparing measurements of CT angiography, TEE, and fluoroscopy of the left atrial appendage for percutaneous closure. *J Cardiovasc Electrophysiol* 2016;27:414-22.
  25. Eng MH, Wang DD, Greenbaum AB, et al. Prospective, randomized comparison of 3-dimensional computed tomography guidance versus TEE data for left atrial appendage occlusion (PRO3DLAAO). *Catheter Cardiovasc Interv* 2018;92:401-7.
  26. Sattar Y, Kompella R, Ahmad B, et al. Comparison of left atrial appendage parameters using computed tomography vs. transesophageal echocardiography for watchman device implantation: a systematic review & meta-analysis. *Expert Rev Cardiovasc Ther* 2022;20:151-60.
  27. Ellis CR. Amplatzer Amulet™ left atrial appendage occluder: a step-by-step guide to device implantation. *J Cardiovasc Electrophysiol* 2022;33:1881-7.
  28. Tzikas A, Bergmann MW. Left atrial appendage closure: patient, device and post-procedure drug selection. *EuroIntervention* 2016;12(Suppl X):X48-54.
  29. Posada-Martinez EL, Trejo-Paredes C, Ortiz-Leon XA, et al. Differentiating spontaneous echo contrast, sludge, and thrombus in the left atrial appendage: can ultrasound enhancing agents help? *Echocardiography* 2019;36:1413-7.
  30. Porter TR, Mulvagh SL, Abdelmoneim SS, et al. Clinical applications of ultrasonic enhancing agents in echocardiography: 2018 American Society of Echocardiography guidelines update. *J Am Soc Echocardiogr* 2018;31:241-74.
  31. Catino AB, Ross A, Suksaranjit P, et al. Improved thrombus assessment by transesophageal echocardiography: the DOLOP (detection of left atrial appendage thrombosis utilizing optison) study. *J Am Soc Echocardiogr* 2021;34:916-7.
  32. Yamashita E, Kemi Y, Sasaki T, et al. Stepwise increase of isoproterenol bolus dose method for differentiating left atrial appendage sludge from thrombus. *J Am Soc Echocardiogr* 2023;36:553-5.
  33. Bhattal GK, Wang Z, Al-Azizi K. Dobutamine-supported WATCHMAN FLX implant in a patient with recurrent left atrial appendage thrombus and spontaneous echo contrast formation. *Proc (Bayl Univ Med Cent)* 2022;35:517-9.
  34. Pandey AC, Shen CP, Chu E, et al. Inotropes to differentiate dense spontaneous echo contrast from thrombus in the left atrial appendage. *JACC Clin Electrophysiol* 2023;9:2655-7.
  35. Fukutomi M, Fuchs A, Bieliauskas G, et al. Computed tomography-based selection of transeptal puncture site for percutaneous left atrial appendage closure. *EuroIntervention* 2022;17:e1435-44.
  36. Saw J, Holmes DR, Cavalcante JL, et al. SCAI/HRS expert consensus statement on transcatheter left atrial appendage closure. *Heart Rhythm* 2023;20:e1-16.
  37. Aminian A, Leduc N, Freixa X, et al. Left atrial appendage occlusion under miniaturized transesophageal echocardiographic guidance and conscious sedation: multicenter European experience. *JACC Cardiovasc Interv* 2023;16:1889-98.
  38. MacDonald ST, Newton JD, Ormerod OJ. Intracardiac echocardiography off piste? Closure of the left atrial appendage using ICE and local anesthesia. *Catheter Cardiovasc Interv* 2011;77:124-7.
  39. Berti S, Paradossi U, Meucci F, et al. Periprocedural intracardiac echocardiography for left atrial appendage closure: a dual-center experience. *JACC Cardiovasc Interv* 2014;7:1036-44.
  40. Zhang ZY, Li F, Zhang J, et al. A comparable efficacy and safety between intracardiac echocardiography and transesophageal echocardiography for percutaneous left atrial appendage occlusion. *Front Cardiovasc Med* 2023;10:1194771.
  41. Berti S, Pastormerlo LE, Santoro G, et al. Intracardiac versus transesophageal echocardiographic guidance for left atrial appendage occlusion: the LAAO Italian Multicenter Registry. *JACC Cardiovasc Interv* 2018;11:1086-92.
  42. Flautt T, Da-Wariboko A, Lador A, et al. Left atrial appendage occlusion without fluoroscopy: optimization by 4D intracardiac echocardiography. *JACC Cardiovasc Interv* 2022;15:1592-4.
  43. Chu H, Du X, Shen C, et al. Left atrial appendage closure with zero fluoroscopic exposure via intracardiac echocardiographic guidance. *J Formos Med Assoc* 2020;119:1586-92.
  44. Zahid S, Gowda S, Hashem A, et al. Feasibility and safety of intracardiac echocardiography use in transcatheter left atrial appendage closure procedures. *J Soc Cardiovasc Angiogr Interv* 2022;1:100510.
  45. Berti S, Santoro G, Brscic E, et al. Left atrial appendage closure using AMPLATZER™ devices: a large, multicenter, Italian registry. *Int J Cardiol* 2017;248:103-7.
  46. Boersma LV, Schmidt B, Betts TR, et al. Implant success and safety of left atrial appendage closure with the WATCHMAN device: peri-procedural outcomes from the EWOLUTION registry. *Eur Heart J* 2016;37:2465-74.
  47. Reddy VY, Möbius-Winkler S, Miller MA, et al. Left atrial appendage closure with the Watchman device in patients with a contraindication for oral anticoagulation: the ASAP study (ASA Plavix Feasibility Study with watchman left atrial appendage closure technology). *J Am Coll Cardiol* 2013;61:2551-6.
  48. Landmesser U, Schmidt B, Nielsen-Kudsk JE, et al. Left atrial appendage occlusion with the AMPLATZER Amulet device: periprocedural and early clinical/echocardiographic data from a global prospective observational study. *EuroIntervention* 2017;13:867-76.
  49. Nestelberger T, Alfadhel M, McAlister C, et al. Follow up imaging after left atrial appendage occlusion-something or nothing and for how long? *Card Electrophysiol Clin* 2023;15:157-68.
  50. Alkhouli M, Alarouri H, Kramer A, et al. Device-related thrombus after left atrial appendage occlusion: clinical impact, predictors, classification, and management. *JACC Cardiovasc Interv* 2023;16:2695-707.
  51. Kar S, Doshi SK, Sadhu A, et al. Primary outcome evaluation of a next-generation left atrial appendage closure device: results from the PINNACLE FLX Trial. *Circulation* 2021;143:1754-62.
  52. Sedaghat A, Vij V, Al-Kassou B, et al. Device-related thrombus after left atrial appendage closure: data on thrombus characteristics, treatment strategies, and clinical outcomes from the EUROOC-DRT-Registry. *Circ Cardiovasc Interv* 2021;14:e010195.
  53. Alkhouli M, Busu T, Shah K, et al. Incidence and clinical impact of device-related thrombus following percutaneous left atrial appendage occlusion: a meta-analysis. *JACC Clin Electrophysiol* 2018;4:1629-37.

54. Dukkipati SR, Kar S, Holmes DR, et al. Device-related thrombus after left atrial appendage closure: incidence, predictors, and outcomes. *Circulation* 2018;138:874-85.
55. Schmidt B, Nielsen-Kudsk JE, Ellis CR, et al. Incidence, predictors, and clinical outcomes of device-related thrombus in the Amulet IDE trial. *JACC Clin Electrophysiol* 2023;9:96-107.
56. Sedaghat A, Nickenig G, Schrickel JW, et al. Incidence, predictors and outcomes of device-related thrombus after left atrial appendage closure with the WATCHMAN device-insights from the EWOLUTION real world registry. *Catheter Cardiovasc Interv* 2021;97:E1019-24.
57. Simard T, Jung RG, Lehenbauer K, et al. Predictors of device-related thrombus following percutaneous left atrial appendage occlusion. *J Am Coll Cardiol* 2021;78:297-313.
58. Fauchier L, Cinaud A, Brigadeau F, et al. Device-related thrombosis after percutaneous left atrial appendage occlusion for atrial fibrillation. *J Am Coll Cardiol* 2018;71:1528-36.
59. Kaneko H, Neuss M, Weissenborn J, et al. Predictors of thrombus formation after percutaneous left atrial appendage closure using the WATCHMAN device. *Heart Vessels* 2017;32:1137-43.
60. Aminian A, Schmidt B, Mazzone P, et al. Incidence, characterization, and clinical impact of device-related thrombus following left atrial appendage occlusion in the prospective global AMPLATZER Amulet observational study. *JACC Cardiovasc Interv* 2019;12:1003-14.
61. Vij V, Piayda K, Nelles D, et al. Clinical and echocardiographic risk factors for device-related thrombus after left atrial appendage closure: an analysis from the multicenter EUROCC-DRT registry. *Clin Res Cardiol* 2022;111:1276-85.
62. Freixa X, Cepas-Guillen P, Flores-Umanzor E, et al. Pulmonary ridge coverage and device-related thrombosis after left atrial appendage occlusion. *EuroIntervention* 2021;16:e1288-94.
63. Cepas-Guillén P, Flores-Umanzor E, Leduc N, et al. Impact of device implant depth after left atrial appendage occlusion. *JACC Cardiovasc Interv* 2023;16:2139-49.
64. Rashid HN, Layland J. Association between device-related thrombus and the neo-appendage with left-atrial appendage occlusion devices. *Eur Heart J* 2021;42:1047-8.
65. Zhong Z, Gao Y, Kovács S, et al. Impact of left atrial appendage occlusion device position on potential determinants of device-related thrombus: a patient-specific in silico study. *Clin Res Cardiol* 2024;113:1405-18.
66. Glikson M, Wolff R, Hindricks G, et al. EHRA/EAPCI expert consensus statement on catheter-based left atrial appendage occlusion - an update. *Europace* 2020;22:184.
67. Main ML, Fan D, Reddy VY, et al. Assessment of device-related thrombus and associated clinical outcomes with the WATCHMAN left atrial appendage closure device for embolic protection in patients with atrial fibrillation (from the PROTECT-AF trial). *Am J Cardiol* 2016;117:1127-34.
68. Korsholm K, Jensen JM, Nørgaard BL, et al. Detection of device-related thrombosis following left atrial appendage occlusion: a comparison between cardiac computed tomography and transesophageal echocardiography. *Circ Cardiovasc Interv* 2019;12:e008112.
69. Kramer AD, Korsholm K, Jensen JM, et al. Cardiac computed tomography following watchman FLX implantation: device-related thrombus or device healing? *Eur Heart J Cardiovasc Imaging* 2023;24:250-9.
70. Miller T, Hana D, Patibandla S, et al. Cardiac computed tomography angiography for device-related thrombus assessment after WATCHMAN FLX™ occluder device implantation: a single-center retrospective observational study. *Cardiovasc Revasc Med* 2022;41:35-46.
71. Iriart X, Blanc G, Bouteiller XP, et al. Clinical implications of CT-detected hypoaattenuation thickening on left atrial appendage occlusion devices. *Radiology* 2023;308:e230462.
72. Alkhouli M, Du C, Killu A, et al. Clinical impact of residual leaks following left atrial appendage occlusion: insights from the NCDR LAAO Registry. *JACC Clin Electrophysiol* 2022;8:766-78.
73. Reddy VY, Holmes DR Jr., Doshi SK. Peri-device leak after left atrial appendage closure: impact on long-term clinical outcomes (abstract 16212). *Circulation* 2021;144:e564-93.
74. Price MJ, Ellis CR, Nielsen-Kudsk JE, et al. Peridevice leak after transcatheter left atrial appendage occlusion: an analysis of the Amulet IDE trial. *JACC Cardiovasc Interv* 2022;15:2127-38.
75. Samaras A, Papazoglou AS, Balomenakis C, et al. Residual leaks following percutaneous left atrial appendage occlusion and outcomes: a meta-analysis. *Eur Heart J* 2024;45:214-29.
76. Hildick-Smith D, Landmesser U, Camm AJ, et al. Left atrial appendage occlusion with the Amplatzer™ Amulet™ device: full results of the prospective global observational study. *Eur Heart J* 2020;41:2894-901.
77. Alkhouli M, De Backer O, Ellis CR, et al. Peridevice leak after left atrial appendage occlusion: incidence, mechanisms, clinical impact, and management. *JACC Cardiovasc Interv* 2023;16:627-42.
78. Korsholm K, Jensen JM, Nørgaard BL, et al. Peridevice leak following Amplatzer left atrial appendage occlusion: cardiac computed tomography classification and clinical outcomes. *JACC Cardiovasc Interv* 2021;14:83-93.
79. Qamar SR, Jalal S, Nicolaou S, et al. Comparison of cardiac computed tomography angiography and transoesophageal echocardiography for device surveillance after left atrial appendage closure. *EuroIntervention* 2019;15:663-70.